Materials Science & Engineering C 114 (2020) 111024

Contents lists available at ScienceDirect

Materials Science & Engineering C

journal homepage: www.elsevier.com/locate/msec

Photocatalytic reduction and anti-bacterial activity of biosynthesized silver nanoparticles against multi drug resistant *Staphylococcus saprophyticus* BDUMS 5 (MN310601)

Govindan Nadar Rajivgandhi[a], Muthuchamy Maruthupandy[b], Jia-Ling Li[a], Lei Dong[a], Naiyf S. Alharbi[c], Shine Kadaikunnan[c], Jamal M. Khaled[c], Khalid F. Alanzi[c], Wen-Jun Li[a,d,*]

[a] State Key Laboratory of Biocontrol, Guangdong Provincial Key Laboratory of Plant Resources and Southern Marine Science and Engineering Guangdong Laboratory (Zhuhai), School of Life Sciences, Sun Yat-Sen University, Guangzhou 510275, PR China
[b] Laboratorio de Nanocelulosa y Biomateriales, Departamento de Ingeniería Química, Biotecnología y Materiales, Facultad de Ciencias Físicas y Matemáticas, Universidad de Chile, Avenida Beauchef 851, Santiago, Chile
[c] Department of Botany and Microbiology, College of Science, King Saud University, Riyadh 11451, Saudi Arabia
[d] State Key Laboratory of Desert and Oasis Ecology, Xinjiang Institute of Ecology and Geography, Chinese Academy of Sciences, Urumqi 830011, PR China

ARTICLE INFO

Keywords:
Food pathogen
Biofilm
Silver nanoparticle
Biofilm inhibition
Photocatalytic activity
Methylene blue

ABSTRACT

In this study, silver nanoparticles (Ag NPs) was eco-friendly synthesized using purified flavonoid rich content of *Morinda citrifolia* (*M. citrifolia*) extract. The synthesized Ag NPs was exhibited at 420 nm in UV-spectrometer, and surface morphology with available chemical composition, shape and size of the Ag NPs were confirmed by X-ray diffraction (XRD) variation, scanning electron microscope (SEM) with energy dispersive X-ray spectroscopy (EDX) and transmission electron microscope (TEM). In addition, the excellent phytochemicals and anti-oxidant activity of the Ag NPs were confirmed by total anti-oxidant and DPPH free radical scavenging assays. Further, the concentration dependent inhibition of synthesized Ag NPs against biofilm forming *Staphylococcus aureus* (*S. aureus*) was confirmed by minimum inhibition concentration (MIC). The growth cells were arrested in the log phase of the culture and detected by flow cytometry analysis. In addition, the bacterial viability, exopolysaccharide degradation, intracellular membrane damage, matured biofilm inhibition, architectural damage and morphological alteration were confirmed by confocal laser scanning electron microscope (CLSM) and SEM. Furthermore, the synthesized Ag NPs reacted with methylene blue (MB) dye molecules has 100% degradation at an irradiation time of 140 min. Conclusively, the eco-friendly synthesized Ag NPs has excellent anti-oxidant, anti-bacterial through intracellular membrane damage, cell cycle arrest and methylene blue dye removal.

1. Introduction

Food born infections are the most important cause for human diseases accounting more numbers of death every year [1]. Infection caused by food born pathogens are more prevalent in China due to the ready-to-eat food products [2]. These food products are prepared in lower thermal, high pressure, UV irradiation, or electric pulse treatment, which might be helped to survive and development of bacteria [3]. Overdue of these preparations compromised for large account of bacterial illness or production of bacterial toxin. Consumption of contaminated food with bacteria cause widespread health problem, being the important food born disease including campylobacteriosis, listeriosis, hemorrhagic colitis and salmonellosis [4]. Recently, Xiao-Hong et al. [5] reported that food born bacteria cause 50 million people every year resulting 7000 death in the China. Among the various bacteria, the genus *Staphylococcus* represents serious food born bacteria, particularly *Staphylococcus saprophyticus* (S. *saprophyticus*). It is an important food born gram positive bacteria (GPB), facultative anaerobic and catalase positive, present in cheese, milk and meats or other environmental sources including soil, water and air [6]. It is considered as one of the most leading causes of food intoxication due to the production of a wide range of heat-stable enterotoxins, as well as toxic shock syndrome toxin type-1 (TSST-1). The control of *S. saprophyticus* is very difficult due to the development of multi drug resistant (MDR) molecules. Various measures are employed now a days to avoid transmission of *Staphylococcus* in food processing and livestock industry [7]. In food industry, *S.*

* Corresponding author at: State Key Laboratory of Biocontrol, Guangdong Provincial Key Laboratory of Plant Resources and Southern Marine Science and Engineering Guangdong Laboratory (Zhuhai), School of Life Sciences, Sun Yat-Sen University, Guangzhou 510275, PR China.
E-mail address: liwenjun3@mail.sysu.edu.cn (W.-J. Li).

https://doi.org/10.1016/j.msec.2020.111024
Received 3 December 2019; Received in revised form 16 April 2020; Accepted 26 April 2020
Available online 28 April 2020
0928-4931/

saprophyticus is big challenge due to the continuous production of virulence factors including efflux pump, QS, biofilm and various enzyme productions [8].

Recent years, Chinese Government continuously implemented a necessary action and plans for aimed to ensuring food integrity including promulgation and revision of the Food Safety Law, as well as the establishment of the State Council Food Safety Committee, the National Food Safety Risk Assessment Center and the China Food and Drug Administration (CFDA) [1,2]. Therefore, an emerging requisite for new therapeutic approaches exists to eradicate the biofilm formation. Numerous reports recommend the use of biosynthesized nanotechnology as promising agents for combating the food borne pathogens.

The synthesis of nanoparticles via biological methods is very reliable and is an alternative to more complex chemical synthetic procedures to obtain nanomaterials. Some of these biological methods include the use of microbes and plants extract [9,10]. Metal nanoparticles are synthesized and stabilized by chemical methods, electrochemical reduction, photochemical reactions, thermal decomposition and also by physical methods for example heat evaporation [11–15]. The NPs synthesized via chemical and physical methods are highly reactive, hazardous and cause potential damage to environment [16]. Therefore, there is a growing need for eco -friendly biomimetic approach for the synthesis of NPs. Biomimetic is an interdisciplinary approach in which NPs are synthesized biologically [17]. A wide variety of biological sources such as plant extracts, microorganisms, enzymes, starch and biopolymers have been utilized by researchers towards greener synthesis of NPs.

Various categories of nanomaterials like metal, metal oxide and polymer NPs have recently arisen from biologically mediated syntheses [18,19]. Among these nanoparticles, Ag NPs were found to be more productive and applied for many applications including antimicrobials, therapeutics, anti-biofilm, anticancer, biomolecular detection, biolabeling, catalysis and microelectronics, nonlinear optics and intercalation materials for electrical batteries [20–23]. Therefore, the present study is aimed to synthesize and characterize the Ag NPs from flavonoid fraction of *M. citrifolia*, and to evaluate its anti-bacterial and photocatalytic activity against food pathogens and methylene blue dye removal.

2. Materials and methods

2.1. Collection of samples

The fresh healthy leaves of *M. citrifolia* were collected from Kolli hills, Namakkal District, Tamil nadu, India. The samples were rinsed with tap water and followed by$D.H_2O$ to remove the contamination and infected leaves and maintained at room temperature for 15 min and then powdered for further experimental usages. The biofilm producing *S. saprophyticus* BDUMS 5 (MN310601) was collected from Department of Marine Sciences, Bharathidasan University, Tiruchirappalli, India.

2.2. Preparation of the extract

500 g powdered plant material was extracted with methanol by using soxhlet method at 37 °C maceration. After, methanol was removed under reduced pressure at 45 °C using a rotary evaporator, and approximately 25% *w*/w yield of sticky dark green crude extract was obtained. The crude extract was mixed with methanol and purified by preparative HPLC attached with perkin Elmer Serious 2000 pump, a Gilson FC203B fraction collector (Shimadzu, Japan) and a perkin Serious 200 UV/VIS detector set at 238 nm for separation of active compounds. The purified extract was evaluated against biofilm forming food pathogen *S. saprophyticus* BDUMS 5 (MN310601) by agar well diffusion method. Amoxicillin acted as a positive control and methanol acted as a negative control [24]. Further, the anti-bacterial potential of purified extract was analyzed by using analytical HPLC for detect the lead compound hits identification (acetonitrile-methanol-ammonium acetate-water (45:10:10:35)) and followed by preparative HPLC for separate the analytical HPLC fractions (C18 column, 150 mm × 4.6 mm, 4.6 μm) using a linear gradient at the flow rate of 1 mL/min at 210 nm). The gradient elution program was 10-90 % and 90-100% at 0-10 min and 11-20 min respectively. Injection volume was 20 μL and column temperature was maintained at 40 °C [25]. Furthermore, all the purified HPLC fractions were separately performed against *S. saprophyticus* BDUMS 5 (MN310601) by agar well diffusion method. Whereas, the third generation chaphalosporin chephalosporin piperacillin/tazobactam acted as a positive control and methanol acted as a negative control. The active fraction of the extract was separately fractionated and scanned by using analytical HPLC. The solvents of the extract were removed by using lyophilization at 40 °C. Finally, the active fraction of the crude compound was obtained and selected for further study.

2.3. Gas chromatography–mass spectroscopy (GC–MS) detection of active fraction

The active fraction of *M. citrifolia* was carried out by using GC–MS (QP5050 a model with GC-17A version, Shimadzu, Germany) analysis for detection of metabolic compounds [26]. In GC–MS analysis, the GBP-5 containing 20 M, 0.22 mM, I.D 0.25 MM thickness of film coated with non-polar column was used. For gas carrier, the ultra-pure helium was used with 70 eV ionization voltage by flow rate of 0.8 mL/Min. The split ratio was 30 and the initial temperature was 260–280 °C and injector were used, respectively. Oven temperature was maintained at 40, 100, 220 and 280 °C at 5 min time interval. The interpretation between mass spectrum and its retention times were detected by Sun Yat-Sen University Library, Guangzhou, China with NIST08, Wiley 9.0 library facility.

2.4. Detection of phenolic compound

According to the Folin–Ciocalteu method, total phenolic content of active fraction was calculated by spectrophotometer using 96-well polystyrene plate [27]. Briefly, 100 mg/mL sample was diluted with 3 mL dist. H_2O and mixed vigorously, followed by added with 0.5 mL Folin–Ciocalteu reagent for 3 min. 20% sodium carbonate (Na_2CO_3) was added into the mixture at 45 °C heat for 10 min. Then, cooled at 37 °C under dark condition for 1 h and then read absorbance at 760 nm by spectrophotometer (Shimadzhu, Japan). The procedure was used three time for triplicate values based on the calculation curve of standard gallic acid. Total phenolic content was suggested as micro grams of gallic acid equal to milligram of dried samples.

2.5. Analysis of flavonoid contents

The rich flavonoid content present in the active *M. citifolia* fraction was confirmed by aluminium chloride colorimetric method [28]. Briefly, 20 μL active *M. citrifolia* fraction was mixed with prepared solution including 700 μL D H_2O, 350 μL ethanol, 25 μL aluminium chloride and 25 μL potassium acetate solutions, and incubated for 30 min in dark room. After, the sample was measured at 415 nm against a blank. Rutin was used as a standard control. Total flavonoid content was recorded as micrograms of rutin that equal to milligram of dried samples. This experiments were conducted in triplicate manner.

2.6. Antioxidant activity

Active fraction of *M. citrifolia* was performed for detect their antioxidant capacity by using phospho molybdenum-based method [29]. 10 μL fraction was mixed with 1 mL prepared solution including sodium phosphate, ammonium molybdate and H_2SO_4 at 97 °C for 1 h in water

bath. After incubation, the OD was measured at 600 nm using biophotometer (Shimadzhu, Japan). Ascorbic acid was acted as a standard control. Anti-oxidant activity was suggested that micrograms of ascorbic acid as equivalents to active fraction.

2.7. 1,1-Diphenyl-2-picrylhydrazyl (DPPH) free radical scavenging assay

Antioxidant effect of active fraction was determined by 1,1-diphenyl-2-picrylhydrazyl (DPPH) assay [30]. Aliquot different concentration of 50 μL active fraction and 3 μL standard control of butylatedhydroxyl toluene were taken in a microtitre plate with 200 μL DPPH in methanol. All the samples were incubated at 37 °C for 30 min in dark condition. Methanol alone was acted as a blank. After incubation, the samples were calculated by UV–vis spectrophotometer (UV-1600, Shimadzu, Japan) at 517 nm with following formula,

$$\text{DPPH scavenged (\%)} = [(\text{Control OD} - \text{Test OD})/\text{Control OD}] \times 100 \quad (1)$$

2.8. Bio-synthesis of Ag NPs

Ag NPs was synthesized by mixing the freshly prepared purified fraction of *M. citrifolia* and freshly prepared 1 mM silver nitrate solution (1:9) at 37 °C for 2 h. After incubation, the alteration of color from white to pale yellow was noted by visible observation. The synthesized solution was centrifuged at 10,000 rpm at 15 min at 4 °C to separate the nanoparticles. Then, the collected sample was air dried and further washed with sterile D H_2O and kept in hot air oven for drying at 45 °C for 24 h. The collected powder was stored in the refrigerator for further use.

2.9. Characterization of Ag NPs

The biosynthesized Ag NPs was primarily confirmed by UV–Vis spectroscopic analysis (UV, Shimadzu-2500, Germany) at the wavelength of 200–800 nm. Powder XRD (XPert PRO, PRO, Analytical, Netherlands, Cu kα radiation, $\lambda = 1.54187^0$ A) was conducted for detection of diffraction intensities at 2θ range from 10^o to 80^o. The accurate Ag NPs morphology was analyzed by using SEM coated with sputter of copper grids and supported by the result of EDX (Hitachi S-4800, Japan). Additionally, the structural intensities of the Ag NPs morphology was imaged by TEM (Shimadzhu, Germany).

2.10. Biological properties of the Ag NPs

2.10.1. Bacterial-inactivation activity

The anti-bacterial activity of the Ag NPs was evaluated against food pathogen *S. saprophyticus* (MN310601) by agar well diffusion method [31]. The overnight culture of *S. saprophyticus* (MN310601) inoculums were swabbed on the surface of freshly prepared Muller Hinton Agar (MHA) plates and 5 mm of wells were cut into the agar. Then, 50 μL Ag NPs was added drop wise into the wells. D H_2O was used as a negative control and piperacillin/tazobactum was used as a positive control. The plate was incubated at 37 °C for 24 h. After incubation, the antibacterial activity of the Ag NPs was measured in terms of the bacteriostatic zone diameter.

2.10.2. Minimum inhibition concentration/minimum bactericidal concentration (MIC)/MBC

The bactericidal activity of Ag NPs against biofilm forming food pathogen *S. saprophyticus* (MN310601) was determined by microbroth dilution method using 96 well plate [32]. 10 μL of bacterial culture was added into the 100 μL of sterile tryptic soy broth containing wells, and different concentrations 10–100 μg/mL of Ag NPs was added into the wells at 37 °C for 24 h. After incubation, the plate wells were monitored for turbidity as growth and non-turbidity as no growth. According to the Clinical and Laboratory Standards Institutes (CLSI) guidelines, the MIC was indicated as the lowest concentration of the Ag NPs, which exhibited clear fluid with no development of turbidity.

Further, aliquot 10 μL of each MIC well cultures on MHA plates. The plate was incubated at 37 °C for 24 h. After 24 h, the plate was observed for detection of MBC. The MBC was determined as the highest dilution of the Ag NPs or same MIC dilution did not produce any single bacterial colony on the MHA plates after 24 h incubation [24].

2.10.3. Cell cycle arrest by flow cytometry

Flow cytometric analysis was performed to identify the bacterial viability and membrane integrity of tested bacterial cells when treated with MIC of Ag NPs at 24 h using specific Live/Dead Bac Light kit (Thermoscientific, Japan) with the following method of Felipe et al. [33]. After the time period, treated bacterial cells were cold centrifuged at 10000 rpm for 15 min and then washed with 1 mL of cold water twice, filtered 1 × PBS (pH 7.5). Add 2 μL of Propidium iodide (PI) into the sample tube and vortexed followed by incubated at 30 °C for 10 min. As same as procedure of untreated bacterial cells in the PBS were acted as a control. After incubation, the inhibition range of treated and untreated cells were interpreted based on the PI absorption of flow cytometer (FACS MoFlo XDP Beckman Coulter). Analysis was performed in CyteExpert 2.1 software (Bruker, Japan).

2.10.4. Biofilm quantification assay

24 well polystyrene plate was used to measure the biofilm inhibition activity of Ag NPs against biofilm forming *S. saprophyticus* (MN310601) with the following method of Kannappan et al. [34]. Initially, 100 μL log phase culture of bacteria was transferred to 1 mL of TSB containing 24-well plate and different concentration 5, 10, 15, 20, 25, 30, 35, 40, 45, 50, 55, 60, 65, 70, 75 μg/ml of Ag NPs was treated with the same wells. Without addition of Ag NPs containing well served as a control. The plate was incubated at 37 °C for 24 h. After incubation, the plate was washed with double D H_2O to remove the non-adherent bacteria. 500 μL of crystal violet (4%) was used to staining of biofilms for 30 min, followed by D H_2O. After 15 min, 95% ethanol was used for extraction of dried crystal violet, and then total biofilm was measured at OD 540 nm. Whereas, the biofilm forming *P. mirabilis* BDUMS 1 (KY617769) acted as a positive control. Without addition of the Ag NPs well acted as a negative control. The percentage of biofilm inhibition was calculated based on the negative and positive control values. All the procedure was applied three times and given formula was used to calculate the percentage of biofilm inhibition, they are

$$\text{PI} = [\text{Control OD 570 nm} - \text{Test OD 570 nm/Control OD 570 nm}] \times 100 \quad (2)$$

2.10.5. Time variation killing assay

The bactericidal effect of the Ag NPs against biofilm forming *S. saprophyticus* (MN310601) was studied at different time interval [35]. Briefly, log phase culture of *S. saprophyticus* (MN310601) inoculated into the Luria-Bertani broth and incubated at 37 °C for 24 h. After proper time interval of lag, log and decline phases, the O.D values of the samples were taken for detection decreased growth. After incubation, the culture was centrifuged at 10, 000 rpm for 30 min and washed with sterile PBS (1%). Then, resuspended in Rosewell park memorial institute (RPMI) 1640 medium with BIC of Ag NPs treatment at 200 rpm of shaking incubator at different time interval (6, 12, 24 and 48 h). After proper time interval, the samples were detected their OD values for inhibition percentages and compared with control using UV–vis spectrometer.

Further, the different time interval of the treated culture was streaked on CRA medium at 37 °C for 24 h for detection of exopolysaccharide production ability. After 24 h, based on the color variation of growing colonies in the CRA plates were reported. For confirmation, the samples of treated *S. saprophyticus* (MN310601) was separately.

2.10.6. Biofilm metabolic activity

2,3-Bis(2-methoxy-4-nitro-5-sulfophenyl)-2H-tetrazolium-5-carboxanilide (XTT) reduction assay was performed to identify the metabolic respiratory activity of the viable cells [36]. The Ag NPs treated or untreated *S. saprophyticus* (MN310601) cells of 6-well plates were washed with 0.01 mol/L PBS solution and resuspended with equal volume of 25 μL of freshly prepared XTT (Macklin, China) solution was added into the well along with standardized fresh menadione acetone solution (Sigma Aldrich, St. Louis, MO, USA). Plates were incubated at 5 h at 37 °C in dark. After incubation, the cells were removed by centrifugation and the supernatant was read at OD 540 nm using ELIZA reader. Sterile PBS along with XTT-menadione mixture solution was served as a blank. All the samples were conducted in triplicate and the result was presented in percentage of inhibition using following formula,

$$\%\text{of inhibition} = 100\,(540\ \mathrm{OD}_{\mathrm{sample}} - 540\ \mathrm{OD}_{\mathrm{control}}) \times 100 \quad (3)$$

The XTT result was further confirmed by enumeration of serial diluted MHA plates result [37]. 10 μL of treated or untreated Ag NP containing XTT wells were streaked on the MHA plates at 37 °C for 12 and 24 h. After incubation, the viable and non-viable colonies were counted.

2.10.7. EPS quantification assay

Production of EPS in the *S. saprophyticus* (MN310601) was quantified by phenol-sulphuric method [38]. After 24 h incubation with or without treatment of Ag NPs, the cell free supernatants were collected and separately by centrifugation at 5000 rpm for 30 min. The pellets were washed twice with PBS for improve the cell free supernatant after incubated along with isotonic buffer (10 mM Tris/HCl, made up of 10 mM EDTA and 2.5% NaCl, pH 8.0) at 4 °C for 24 h. After incubation, the cell suspension was vortexed for 15 min and centrifuged at 5000 rpm for 35 min. The polysachharide was quantitatively precipitated by drop wise addition of cold absolute alcohol at the ration of (1:1) and kept overnight at −20 °C. Then, sample was re-centrifuged for polysaccharides collection and followed by distilled water. Sample was digested with 5 mL of 98% H_2SO_4 into monosaccharides with continuous stirring. In addition, 1 mL of 5% phenol was added to resulting mixture with stirring in a boiling water bath at 100 °C for 20 min. The mixture was cooled on ice and OD measured at 485 nm by UV–VIS spectrophotometer (UV-5550, Shimadzu, Germany). Sterile D H_2O was served as a blank. The experiment was conducted in triplicate and result of EPS inhibition was indicated in percentage mode using following equation,

$$\%\text{of inhibition} = 100 - \mathrm{Ca/Cb} \times 100 \quad (4)$$

where Ca is concentration of EPS in the samples group, and Cb is concentration of the EPS in the control group.

2.10.8. Live/dead cell differentiation

Intracellular damage effect of Ag NPs against *S. saprophyticus* (MN310601) was visibly detected by CLSM [31]. After incubation with Ag NPs treated or untreated cultures were sediment by centrifugation and re-suspended with 100 μL of PBS. Aliquot 0.1 μL of the culture was added on the cover glass and stained by live/dead staining bacterial viability Kit (Live/dead ® BacLight™, Shimadzu, Japan) using SYTO9 green fluorescent dye (0.8 μM) and propidium iodide (PI) red fluorescent dye (10 μM) at dark condition. After incubation, the cover glasses were analyzed under CLSM for detection of live/dead cells at emission wave length of 480–600 nm (CLSM, LSM 710, Carl Zeiss, Jena, Germany).

2.10.9. Morphological damage by SEM and TEM

The morphological damage of Ag NPs treated *S. saprophyticus* (MN310601) (MN310601) was determined by SEM and TEM [34]. After 24 h incubation, the control and treated cells were separately sedimented by centrifugation at 5000 rpm for 30 min and washed with 10 mM sodium phosphate buffer (pH 7.4). Then, the cells were diluted with fresh PBS and fixed on cover slip with an equal volume of 4% glutaraldehyde for 4 h at room temperature followed by two times washed with fresh PBS. The fixed cells were vacuum filtered by 0.1 mm polycarbonate membrane filters and dehydrated in ethanol-graded series (50, 60, 70, 80, 90 and 100%). Cover slip was allowed to dried and mounted on aluminium specimen support and coated with 15 nm thickness of gold-palladium metal (60:40 alloys). The air dried samples were freeze dried at deep freezer for 24 h. After freeze drying, the samples were observed under SEM using an accelerating voltage of 20 kV (VEGA3 TESCAN, Brno, Czech Republic) and TEM (H-7650, Hitachi, Japan) at an operating voltage of 80 kV.

2.10.10. Analysis of biofilm damage

Visualization of damaged biofilm structure of *S. saprophyticus* in the BIC of Ag NPs was observed by CLSM [32]. Briefly, *S. saprophyticus* (MN310601) treated or untreated cultures were allowed to grow on glass slide of 6-well plates at 37 °C for 24 h. All the cover glasses were washed with sterile PBS and stained with acridine orange (0.1% w/v) solution. After 5 min with dark condition, the stained biofilms slides were imaged under CLSM (LSM 710, Carl Zeiss, Oberkochen, Germany).

2.10.11. Mature biofilm damage

The architectural damage of Ag NPs treated *S. saprophyticus* (MN310601) biofilm was analyzed by CLSM using propidium iodide (PI) and 4′,6-diamidino-2-phenylindole (DAPI) staining assay [31]. Briefly, *S. saprophyticus* (MN310601) culture was added into the TSB of 1 × 1 cm glass slide soaked 24 well polystyrene plate and allowed to form biofilm at 37 °C for 12 h incubation. After incubation, the BIC of Ag NPs were added into the treated well and incubated at 37 °C for 12 h. At end of the incubation, the glass slides were washed with sterile PBS and allowed to air dried for 5 min. After, the slides were stained with equal quantity of PI and DAPI and maintained with 15 min dark condition. Finally, the Ag NPs treated and untreated cells were imaged under CLSM (Olympus BX 40, Japan) at 4000× magnification.

2.10.12. Photocatalytic activity

The photocatalytic properties of the prepared Ag NPs was estimated by monitoring the photocatalytic degradation of Methylene Blue (MB) in UV–Vis spectrophotometer (Shimadzu UV-2450). In each experiment, 50 mg of photocatalyst was dispersed in 100 mL of MB aqueous solution (1×10^{-5} M). The suspension was then magnetically stirred in dark for 30 min. Later, the solution was transferred to flask and exposed to the visible light irradiation at a regular time interval of 15 min. After the time interval, the photocatalytic degradation process was monitored using a UV–Vis spectrophotometer to record the characteristic absorption peak at 660 nm of MB [39].

3. Result and discussion

3.1. Purification of active metabolites

The anti-bacterial activity of *M. citrifolia* purified HPLC fractions exhibited 6, 10 and 18 mm zone of inhibition against *S. saprophyticus* at 10, 25 and 50 μg/mL was observed, respectively (Fig. 1c). Further, the anti-bacterial components of the purified HPLC fraction was exhibited with 12 different peaks by analytical HPLC (Fig. 1a) based on the retention time, surface area, area of height and percentages. Among the 12 peaks, peak 3, 7 and 9 exhibited 4, 14 and 22 mm zone of inhibition against *S. saprophyticus* was observed at 50 μg/mL, respectively. Whereas, the third generation chephalosporin was exhibited only 4 mm zone of inhibition (Fig. 1d). The result was suggested that the *S. saprophyticus* as MDR bacteria. These three peak were purified separately and confirmed by analytic HPLC (Fig. 1b). The exhibited result was confirmed that the third fraction has excellent anti-bacterial activity than other two peaks also clearly observed (Fig. 1e). Therefore, the

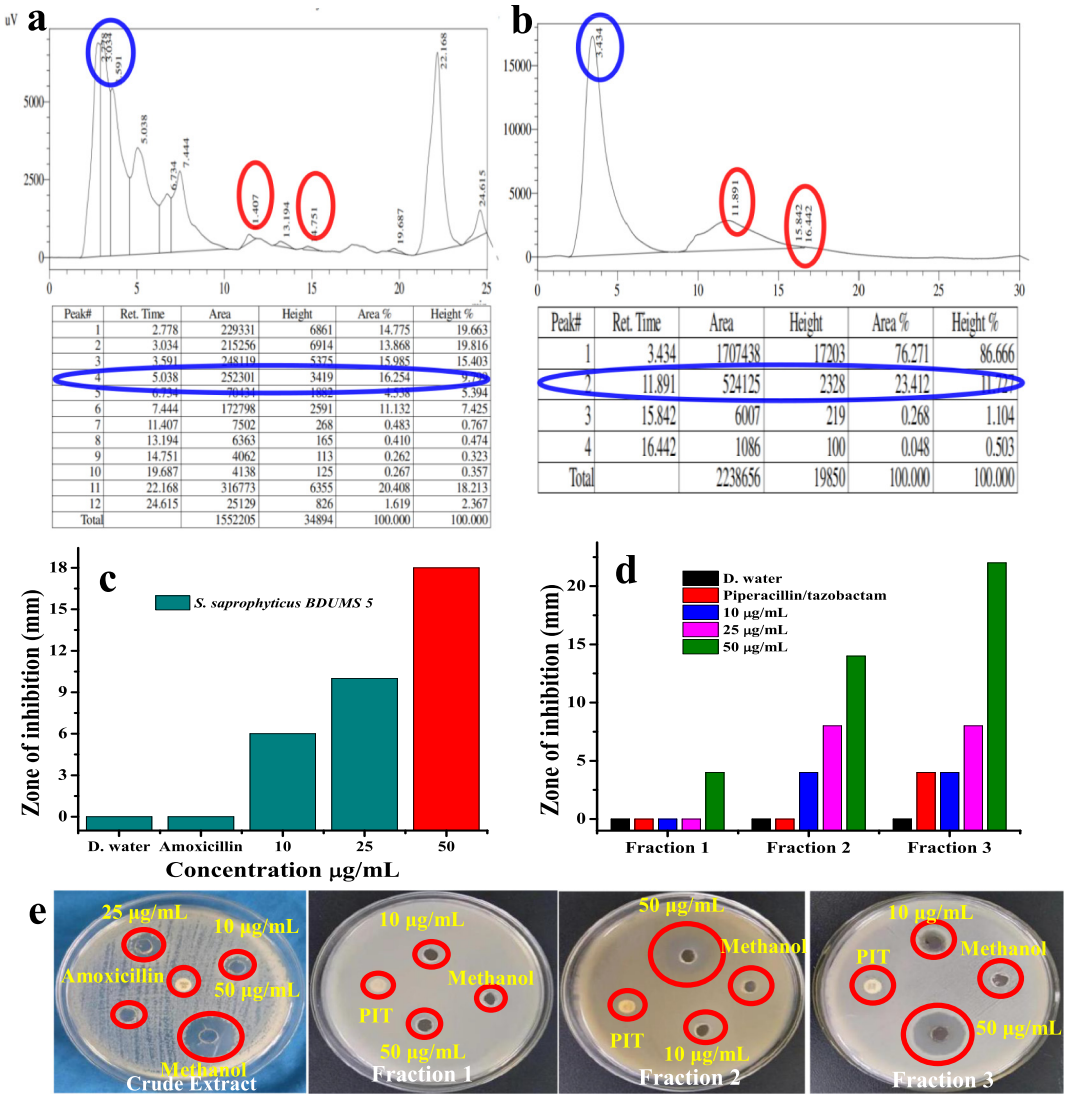

Peak#	Ret. Time	Area	Height	Area %	Height %
1	2.778	229331	6861	14.775	19.663
2	3.034	215256	6914	13.868	19.816
3	3.591	248119	5375	15.985	15.403
4	5.038	252301	3419	16.254	9.797
5	6.734	78434	1882	4.538	5.394
6	7.444	172798	2591	11.132	7.425
7	11.407	7502	268	0.483	0.767
8	13.194	6363	165	0.410	0.474
9	14.751	4062	113	0.262	0.323
10	19.687	4138	125	0.267	0.357
11	22.168	316773	6355	20.408	18.213
12	24.615	25129	826	1.619	2.367
Total		1552205	34894	100.000	100.000

Peak#	Ret. Time	Area	Height	Area %	Height %
1	3.434	1707438	17203	76.271	86.666
2	11.891	524125	2328	23.412	11.727
3	15.842	6007	219	0.268	1.104
4	16.442	1086	100	0.048	0.503
Total		2238656	19850	100.000	100.000

Fig. 1. Analytical HPLC fractions of purified *M. citrifolia extract* and active anti-bacterial fraction (a, b). Anti-bacterial activity differentiation of crude *M. citrifolia* extract (c), differentiation of three purified fractions (d) and agar well diffusion result against S. *saprophyticus*.

present result was suggested that the plant *M. citrifolia* could play an effective role against biofilm producing *S. saprophyticus.*

3.2. GC–MS analysis

The GC–MS analysis of active fraction 3 exhibited 65 major compounds, which carefully identified by NIST library database of Sun Yat-Sen University. The result was confirm, more number of flavonoid derivatives were present in the fraction 3 and this constituents may have anti-bacterial effect against tested bacteria. Among the 65 compounds, flavonoid rich *M. citrafolia* compounds were screened based on the previous report (Table-1), and indicated in inset table of Fig. 2. Resulted compounds and their functional groups were participated into the redox reaction of NPs synthesis as reducing agents. The result was agreed by recent study of Maxine Swee et al. [39] and Zhang et al. [40], flavonoid fraction synthesized Ag NPs has more inhibition against MDR bacteria. Similar studies of Thatoi et al. [41] and Muthupandian et al. [42] reported the *M. citrifolia* mediated Ag NPs could inhibit the MDR of GPB and GNB effectively. Hence, the result was suggested that the flavonoid rich content was present in the plant *M. citrifolia* and it has more bactericidal property. Based on the previous report, the possibilities of the *M. citrifolia* produced compounds were available in Table 1.

3.3. Total phenol and flavonoid content

Based on the standard curve of gallic acid (R^2 = 0. 9782), the total phenolic content was very high in the fraction 3 of *M. citrifolia* (Fig. 2b). The observed phenolic contents with 25–250 µg/mL are markedly very higher than that commonly identified for other plants. In addition, the standard value curve of rutin (R^2 = 0.9997) suggested that the flavonoids contents are also more abundant. The calibration curve was started from 25 to 250 µg/mL (Fig. 2c). Therefore, both the evidence of phenol and flavonoid contents were proved that the fraction 3 of *M. citrifolia* has more phenol and flavonoid contents instead of total sugar and total protein. Our result was agreed with previous studies of Subramaniam [43] and Bittova et al., [44], reported that the *M. citrifolia* has more anti-oxidant and anti-cancer activity due to the rich sources of phenol and flavonoid.

3.4. Antioxidant activity

Based on the rich contents of phenol and flavonoids, we have chosen the *M. citrifolia* extract for anti-oxidant properties and other studies. Interestingly, the fraction 3 was exhibited with more anti-oxidant compared with biosynthesized Ag NPs. Differentiation between leaf extract, Ag NPs and control of ascorbic acid were effectively showed in

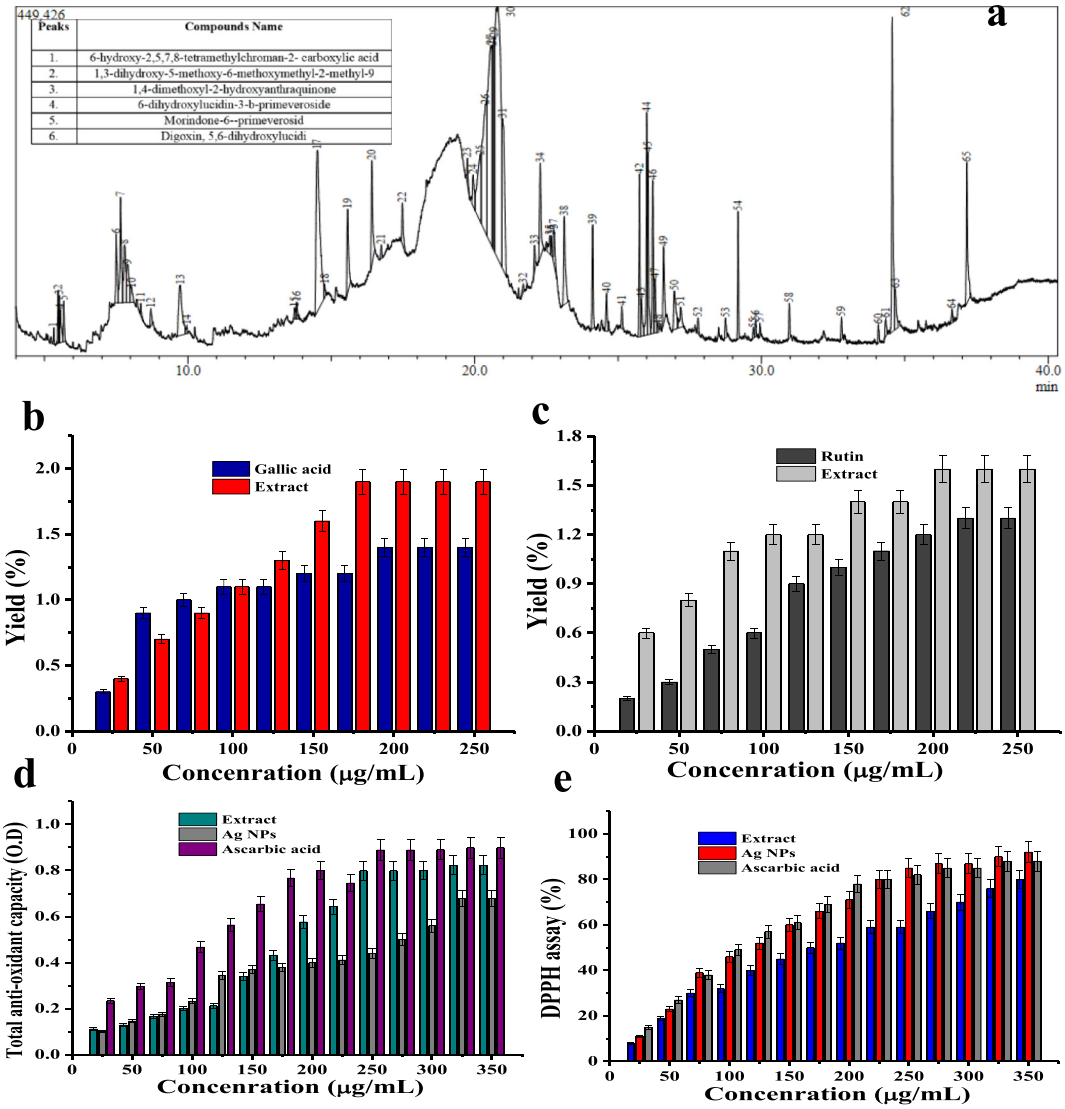

Fig. 2. GC–MS analysis of possible anti-bacterial compound present in the *M. citrafolia* active fraction (a) total phenolic (b), flavonoid contents (c) total anti-oxidant activity (d) and DPPH assay (e) of the HPLC purified *M. citrafolia* fraction 3.

Fig. 2d. The values were noted based on the direct relationship between concentration of the samples and anti-oxidant values. After the time interval, 0. 80, 0. 67 and 0. 88 values were received against crude extract, Ag NPs and ascorbic acid at 350 µg/mL. The exhibited result was suggested that the extract value was closely related to control value when compared with Ag NPs at increasing concentration. Further, the DPPH assay was exhibited 70, 76, 89% of radical scavenging activity against fraction 3, Ag NPs and ascorbic acid at 350 µg/mL. Interestingly, the result was indicated that the Ag NPs has better activity than fraction 3. Contrary, ascorbic acid was higher than that of Ag NPs (Fig. 3e). Result of fraction 3 and Ag NPs was agreed that the plant mediated Ag NPs enhance theanti-oxidant and DPPH free radical scavenging activity than fraction 3 due to the activation of phenol and flavonoid respiration genes [28]. Previous report of Anitha et al. [45] indicated with similar result (50% and 65%). In bacteria, ROS and RNS are most important, which influence the active molecules including lipids, proteins, carbohydrates and nucleic acids in living organisms [38].

3.5. Synthesis and characterization of biosynthesized Ag NPs

The changed color from light green to yellow suggest, the reduction of Ag^{+} to Ag^{0} (Inset figure), and this result indicates confirmation of Ag NPs. The observed reduction of Ag^{+} can be revealed to the action of phytochemical constituents present in the extract. Following successful centrifugation, the surface plasmon resonance (SPR) of the sample was exhibited around 400–420 nm by UV-spectrometer for Ag NPs at a desired concentration to aqueous extract of *M. citrifolia* (Fig. 3a). The exhibited SPR peak's position and shape depend on the particle size and shape of the Ag NPs. According to the MiO theory, the exhibited single sharp peak around 420 nm corresponded to spherical shape of the Ag NPs [46]. The optical properties of metallic NPs depend mainly on its SPR, where the plasmon refers to the collective oscillation of the free electrons within the metallic NPs [47]. The oscillation of electrons in plasmon band depends much on the size, shape, morphology, surface-adsorbed species, composition, and dielectric environment of the prepared NPs [48]. The SPR of Ag NPs tends to shift to longer wavelengths with increasing PS. Pal et al. [49] reported that only a single SPR band is expected in the absorption spectra of spherical NPs, whereas anisotropic particles could give rise to two or more SPR bands depending on the shape of the particles. Thus, the spherical NPs, disks, and triangular nanoplates of silver show one, two, and more peaks, respectively [23].

Powder XRD pattern of Ag NPs was confirmed their purity and crystalline nature of the synthesized Ag NPs in Fig. 3b. In the XRD

Table 1
Total components of active fraction of *Morinda citrafolia* by GC–MS analysis.

Peak	Retention time	Start time	End time	m/z	Area	Area %	Height	Height %	A/H	Name
1	5.475	5.44	5.495	TIC	138,413	0.52	68,103	1.18	2.03	2-Butyl-(2-Methylbutylidene)-Amine
2	5.512	5.495	5.535	TIC	121,073	0.46	61,286	1.06	1.98	n-[4-Aminobutyl]aziridine
3	5.55	5.535	5.64	TIC	136,470	0.51	42,633	0.74	3.2	4-Pyranone, 2,3-dihydro-
4	5.672	5.64	5.74	TIC	122,056	0.46	52,679	0.91	2.32	Methyl 2-Amino-3-Methylbutanoate Hydrochloride
5	7.498	7.45	7.57	TIC	288,301	1.09	88,355	1.53	3.26	Epi-dihydrocornin
6	7.655	7.57	7.725	TIC	521,376	1.96	135,675	2.35	3.84	1-Butanamine, 2-Methyl-n-(2-Methylbutylidene)-
7	7.787	7.725	7.855	TIC	393,782	1.48	73,938	1.28	5.33	2(3h)-Furanone, Dihydro-3-Hydroxy-4,4-Dimethyl-, (.+/−.)-
8	8.045	7.98	8.115	TIC	109,955	0.41	17,513	0.3	6.28	Nicotifloroside
9	8.36	8.33	8.445	TIC	34,370	0.13	15,639	0.27	2.2	Citrifolinin B Epimer A
10	8.711	8.675	8.77	TIC	72,061	0.27	22,483	0.39	3.21	2-Pyrrolidinone
11	9.74	9.625	9.91	TIC	552,913	2.08	64,421	1.12	8.58	Benzeneethanamine
12	9.965	9.91	10	TIC	33,163	0.12	10,908	0.19	3.04	Pentanedioic acid, Dimethyl ester
13	13.725	13.685	13.77	TIC	47,551	0.18	14,174	0.25	3.35	Epi-dihydrocornin
14	13.791	13.77	13.835	TIC	53,675	0.2	21,332	0.37	2.52	1-Acetyl-3-amino-4-cyano-3-pyrroline
15	14.511	14.425	14.74	TIC	1,877,333	7.07	207,799	3.6	9.03	Deacetylasperuloside,
16	14.775	14.74	14.815	TIC	52,819	0.2	16,199	0.28	3.26	Dehydromethoxygaertneroside
17	15.571	15.51	15.675	TIC	390,658	1.47	107,362	1.86	3.64	5-Oxo-pyrrolidine-2-carboxylic acid
18	16.413	16.365	16.51	TIC	465,132	1.75	133,891	2.32	3.47	Alpha-hydroxyadoxoside
19	16.742	16.695	16.795	TIC	45,940	0.17	17,602	0.31	2.61	2-Pyrrolidinone, 5-(cyclohexylmethyl)-
20	17.477	17.44	17.58	TIC	177,889	0.67	53,235	0.92	3.34	Borreriagenin,
21	19.744	19.71	19.825	TIC	87,813	0.33	33,302	0.58	2.64	3-Methyl-4-phenyl-1 h-pyrrole
22	19.944	19.9	20.015	TIC	184,247	0.69	40,575	0.7	4.54	Asperuloside
23	20.19	20.015	20.225	TIC	726,013	2.74	84,332	1.46	8.61	Nitric acid,Pentyl ester
24	20.37	20.225	20.435	TIC	1,765,843	6.65	163,509	2.83	10.8	l-Narcissoside
25	20.565	20.435	20.61	TIC	2,406,180	9.07	255,414	4.43	9.42	Pyrimido[1,2-*a*]azepine, 2,3,4,6,7,8,9,10-octahydro-
26	20.625	20.61	20.64	TIC	465,754	1.75	258,730	4.48	1.8	n-1,3-Butadienyl-2-piperidinone
27	20.67	20.64	20.7	TIC	977,430	3.68	273,595	4.74	3.57	Benzeneethanamine, n,.alpha.,.alpha.-trimethyl-
28	20.807	20.7	20.945	TIC	4,241,491	15.98	324,144	5.62	13.09	D-Valine
29	20.975	20.945	21.11	TIC	1,193,562	4.5	193,160	3.35	6.18	Dl-Isoleucine
30	21.69	21.625	21.72	TIC	36,919	0.14	11,263	0.2	3.28	1,2,5-Oxasilaborolane, 4,4,5-triethyl-2,2,3-trimethyl-
31	22.09	22.04	22.125	TIC	91,234	0.34	31,909	0.55	2.86	Gephyrotoxin 235b′
32	22.285	22.23	22.39	TIC	418,345	1.58	120,822	2.09	3.46	3-Methyl-1,4-diazabicyclo[4.3.0]nonan-2,5-dione, *n*-acetyl-
33	22.616	22.53	22.65	TIC	100,285	0.38	23,581	0.41	4.25	(3s,6s)-3-Butyl-6-methylpiperazine-2,5-dione
34	22.678	22.65	22.715	TIC	54,949	0.21	25,877	0.45	2.12	3-Methoxy-9, H-carbazole
35	23.122	23.06	23.255	TIC	492,648	1.86	113,719	1.97	4.33	Pyrrolo[1,2-*a*]pyrazine-1,4-dione, hexahydro-

spectra, the diffraction peaks at 2θ = 32.06°, 38.03°, 47.18°, 59.33° and 77.18° were corresponded to the diffraction planes of (111), (200), (220) and (311) respectively. The XRD result was compared with the standard JCPDS file No. 04-0783 [50]. The sharp and narrow diffraction peaks of XRD spectrum was indicated that the synthesized Ag NPs was pure and highly crystalline nature [51].

The SEM analysis of Ag NPs was detected to be extremely agglomerated, probably an artefact of the centrifugation and consequent drying essential to synthesized Ag NPs samples for SEM analysis. The Ag NPs characteristically exhibition an absorption peak about 3 keV owed to their surface plasmon resonance [52]. Also the analysis of Ag NPs established a strongly well-defined Ag indication at 3 keV along with weak carbon, oxygen and nitrogen peaks, with the concluding weaker peaks possibly demonstrating surface biomolecule covering morphology inventing from the *M. citrifolia* plant extract Fig. 3c, d. EDX result was indicated that the strong highest peak at Ag NPs region, which confirms the formation of elemental silver (Fig. 3e). Further, the morphological observation of biosynthesized Ag NPs was confirmed by TEM, which revealed that the size of Ag NPs was in range between 10 and 100 nm along with spherical morphology (Fig. 3f, g). In addition, distribution of particle size further suggested that most of Ag NPs possess a 35 nm diameter size, demonstrating that seaweed permits obtaining a smaller Ag NPs with potentially high surface area.

3.6. Bacterial inactivation assay

After 24 h incubation, 10, 25 and 50 μg/ml concentration of Ag NPs exhibited 10, 22 and 34 mm zone of inhibition against *S. saprophyticus* (MN310601) was observed, respectively. Whereas, the negative control well of D.H_2O and positive control well of piperacillin/tazobactum exhibited no zone of inhibition were also observed (Fig. 4a, b). In mechanistic approach, Ag NPs was interact with surface of bacteria and interfere the extracellular polysachharide, nucleic acid DNA, and proteins. Intracellular damaging ability of bacterial virulence and their enzyme synthesized effect was arrested. Similar results were reported by Rufen et al. [53] and Ayse et al. [54], which indicated 16 and 18 mm zone of inhibition against GPB and their enzyme production genes were inactivated at lowest concentration.

3.7. MIC/MBC

In the MIC value of Ag NPs was exhibited concentration-dependent inhibition against *S. saprophyticus* (MN310601) (Fig. 4c). The MIC value of 50 μg/mL concentration was exhibited stronger bacterial growth inhibitory activity towards *S. saprophyticus* (MN310601), and their inhibition percentage was 94% for 24 h. Based on the biosynthesized Ag NPs of previous report, our resulted concentration was very low and the differentiation was available in Table 2. The absorbance result was decreased along with increasing concentration of Ag NPs for tested *S. saprophyticus*. The initial inhibition of 7% and half inhibition of 50% was observed at 5 μg mL and 30 μg/mL, respectively. Further, the MBC result was exhibited same as MIC was also observed (Fig. 4d). The result indicated that the introduction of Ag^+ ion into the bacterial surface could damage when compare to the untreated control. The anti-bacterial activity of Ag NPs and its chemical reactions are attributed to their positively charged Ag^+ group, which interfered the bacterial membrane permeability, alter the bacterial native cell wall structure and damage the cell wall leads to leakage of cell walls [29,55]. This agrees excellent with the disc diffusion assay results. Therefore, the result was indicated that the Ag NPs have excellent antibacterial activity at increasing concentrations and their efficiency was destroy the mechanistic role of *S. saprophyticus*.

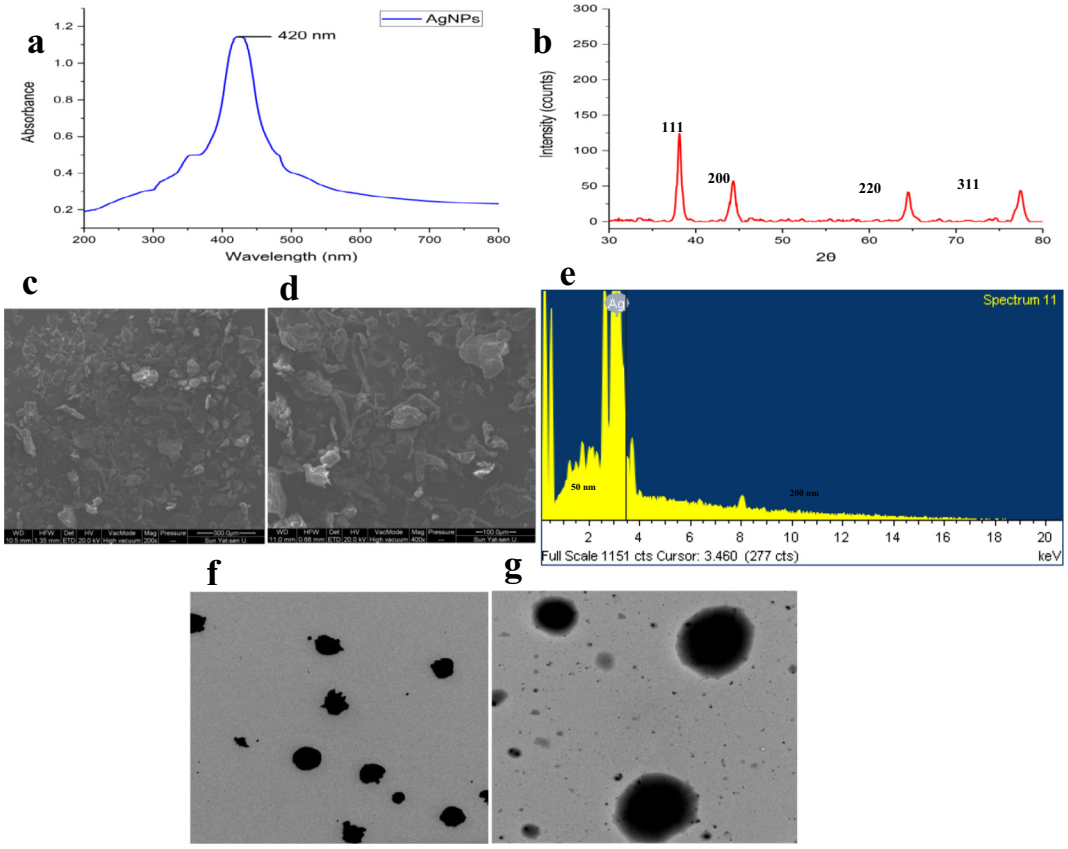

Fig. 3. UV–Vis spectra (a), XRD pattern (b), low and high magnification SEM images showing spherical morphology of Ag NPs (c, d), EDX spectra (e) and TEM morphological identification (f, g) of Ag NPs from flavonoid fraction of *M. citrafolia*.

3.8. Cell cycle arrest by flow cytometry

The *in vitro* inhibition assay of viability was indicated false positive result due to the virulence factors stimulation, while they remain dormant and reproduced enzyme activity after certain period of time [56]. To overcome this problem, the killing efficiency of Ag NPs against tested bacterial cells, especially MIC treated cells were stained with live/dead stains and examined flow cytometry which provided a real time assessment of bacterial viability [34]. On the basis of the staining profile, the entire region of the places were covered with PI observed live and dead bacterial cells, indicating a shift of arranged peak in P1. The percentages differentiation of PI absorbance in dead, and live cells were highlighted in the P2 region. Inhibition range of the dead cells were also observed in P3 region due to the decreased growth of the bacteria. Fig. 5b (PI, P2 and P3) of the scatter plot was indicated that the cells were significantly stained with PI and 98% of the cells were died due to the effect of Ag NPs. Whereas, the tightly arranged cells of P1, P2 and P3 of Fig. 5a indicated that the cells were not observed the PI dye properly and exhibited with well developed bacterial growth. The result was clearly confirmed that the Ag NPs has excellent anti-bacterial activity against MDR *S. saprophyticus*.

3.9. Biofilm quantification assay

In this study, the purified flavonoid rich fraction 3 was used for assessing the anti-biofilm activity and result exhibited complete biofilm inhibition against tested bacteria. The result indicated that the Ag NPs have neither anti-bacterial and anti-biofilm activity at the increasing concentration when compared to control. Initially, Ag NPs showed decreased growth inhibition at 10 μg/mL concentration and half inhibition at 30 μg/mL concentration were observed. In addition, the highest biofilm inhibition (96%) was recorded against selected *S. saprophyticus* (MN310601) at 60 μg/mL (Fig. 6a). Among the few available reports on anti-biofilm activity of food pathogens, biosynthesized Ag NPs revealed promising anti-biofilm properties between 90 and 98% against food borne pathogens [35]. The confirmed evidence of this study result was proved that the flavonoid rich Ag NPs has excellent anti-biofilm activity at 60 μg/mL and this concentration was fixed as a BIC. Further, the crystal violet staining result exhibited, the rigidity of the biofilm structure was degraded at the same concentration when compared with untreated control (Inset Fig. 6a). The Ag NPs inhibit the biofilm forming *S. saprophyticus* (MN310601) through extracellular polysaccharide matrix, which acts as a protective layer around the bacterial colonies. Previous reports of concentration dependent biosynthesized Ag NPs against various MDR and biofilm producing bacteria results were mentioned in Table. 2.

3.10. Time variation killing assay

Based on the different time interval, the complete inhibition of BIC treated *S. saprophyticus* (MN310601) was observed at 24 h. In this stage, cells were under went to decline phase from exponential phase and viability of the cells showed 0%. The remarkably rapid killing effects and absence of doubling time was observed due to the interactions Ag^+ ions into bacterial surfaces. When compared with 6 and 12 h incubation, faster rate of killing, and superior efficacy was observed at 24 h. This increased kill rate and efficacy might contribute Ag^+ to surface channels of charged cell wall surface of the bacteria. The inhibition percentages of *S. saprophyticus* (MN310601) exhibited 94, 72, 48, 35% for 24, 12, 6 and 3 h, respectively. In addition, the concentration-dependent anti-bacterial effect could be clearly observed from Fig. 6b. Further, loss of exopolysaccharide production in the treated *S. saprophyticus* (MN310601) was confirmed in the CRA medium due to the absence of black color when compared with control at increasing time

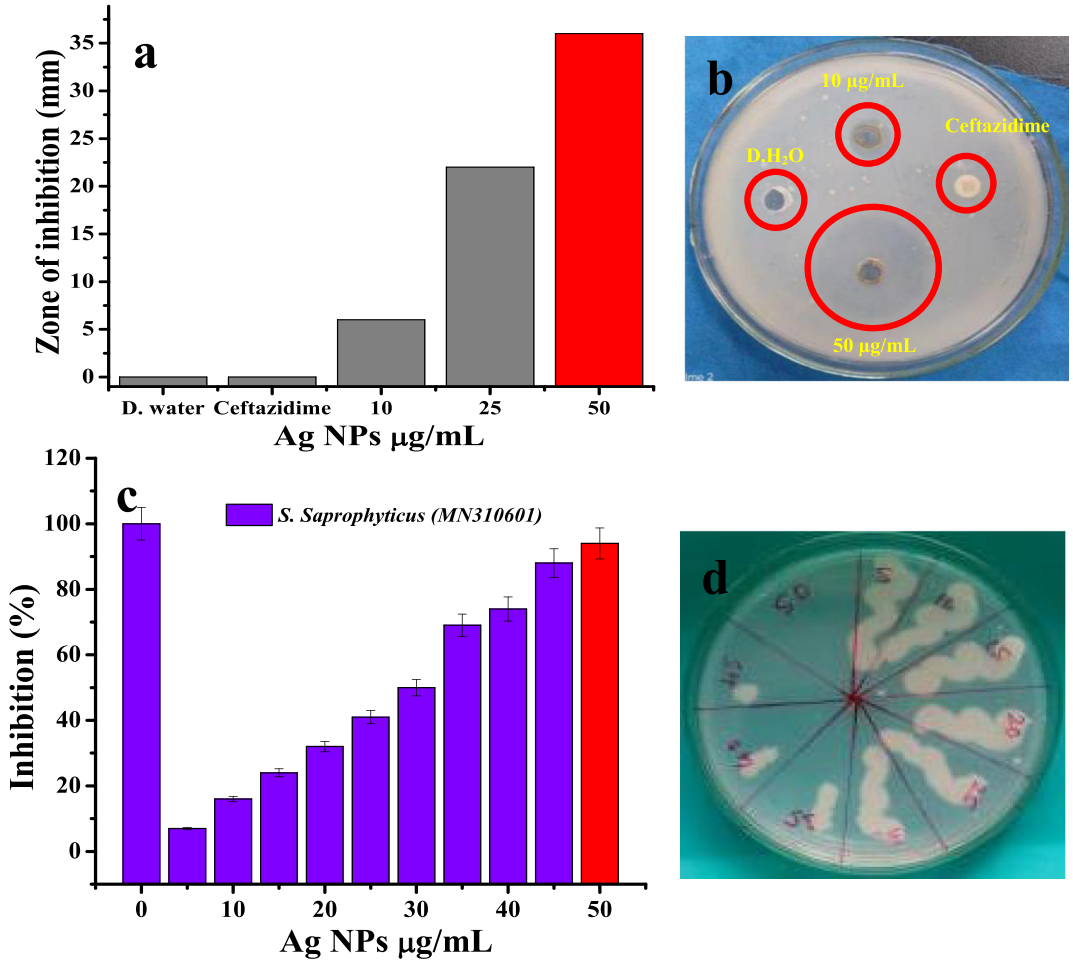

Fig. 4. Agar well diffusion (a, b) and MIC, MBC (c, d) of Ag NPs against *S. saprophyticus* at different concentration.

interval (Inset Fig. 6b). Recently, Pratik et al. [57] and Steff, et al. [58] documented that the BIC of biosynthesized Ag NPs effective against *E. coli*, *P. aeruginosa* and *K. pneumoniae* at 10, 50, and 100 mg/mL. In addition, actinomycete mediated Ag NPs against *S. aureus* was inhibited at 100 µg/mL also supported this study [37].

3.11. Biofilm metabolic assay

A significant decrease of biofilm cells were observed in the treated *S. saprophyticus* (MN310601) biofilm at increasing concentration, while no any decreasing effect of XTT conversation was observed in the untreated control sample (Fig. 6c). Increasing concentration of Ag NPs led to a decrease of viability due to the formazan production. The half viability (54%) and complete viability (95%) was observed at 35 µg/mL and 65 µg/mL. It was clearly indicated that the Ag NPs has considerable reduction ability against *S. saprophyticus* (MN310601).

Further, the absence of bacterial growth at 65 µg/mL concentration streaked MHA plate was also confirmed that the Ag NPs has bactericidal activity (Inset Fig. 6c). The result was agreed with Suma et al. [59], reduced metabolic activity of Ag NPs was interfere the formation of nucleic acid, DNA and other extra cellular products. Recently, Huang et al. [38] reported that the biosynthesized Ag NPs has bactericidal activity against GNB at increasing concentration. Reduction of metabolic activity was caused the QS activation, biofilm formation and

Table 2
Previous reports of concentration dependent biosynthesized Ag NPs against multi drug resistant and biofilm producing bacteria.

S. no	Biosynthesized samples	Test organisms	Concentration (µg/mL)		References
			Anti-bacterial activity	Anti-biofilm activity	
1	Ag NPs	*S. aureus* and *P. aeruginosa*	16	1000	Feizi, Taghipour, Ghadam, & Mohammadi, 2018
2	Ag NPs	*L. monocytogenes* and *V. parahaemolyticus*	50	75	Vijayakumar, Malaikozhundan, Ramasamy, & Vaseeharan, 2016
3	Ag NPs	*S. aureus*	50	55	Rajivgandhi et al., 2019
4	Ag NPs	*E. faecalis* and *A. hydrophila*	100	100	Malaikozhundan, Vaseeharan, Vijayakumar, Sudhakaran, & Gobi, Shanthini, 2016
5	Ag NPs	*K. pneumoniae* (700603), and *E. coli*	16, 50	50	Neihaya, Zaman (2018)
6	Ag NPs	*E. coli* and *S. aeruginosa*	1000	1000	Arya (2019)
7	Ag NPs	*E. faecalis* and *P. aeruginosa*	100	100	Anjugam, et al. (2018)
8	Ag NPs	*S. saprophyticus*	50	60	Current study

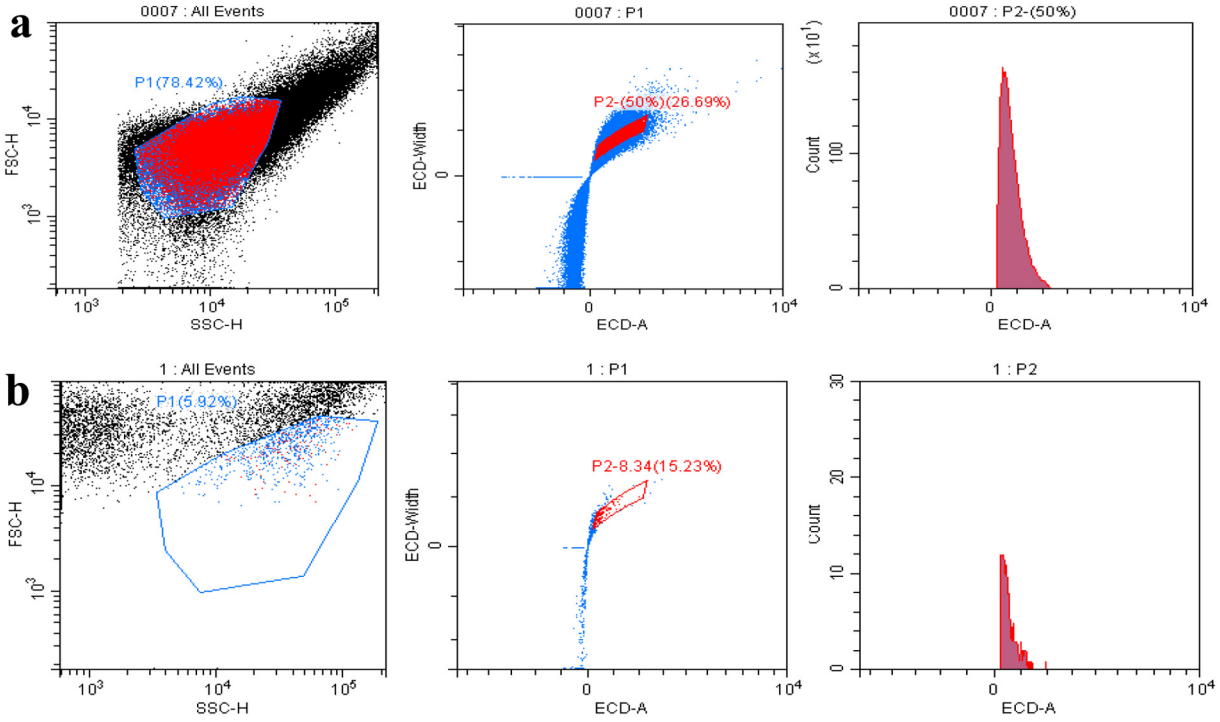

Fig. 5. The cell cycle arrest of *S. saprophyticus* at MIC of Ag NPs by flow cytometercontrol cells (a) and treated cells (b).

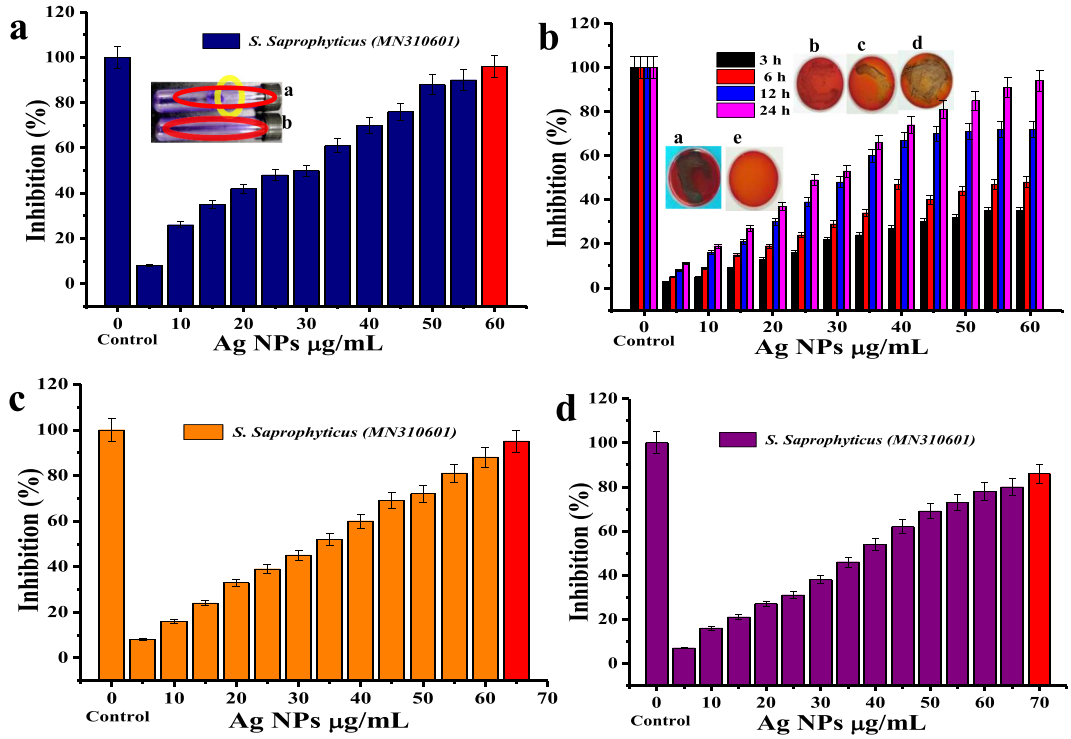

Fig. 6. The anti-biofilm inhibition (a) (Inset Fig. 5a indicated the rigidity and non-rigidity of biofilm ring (a, b)), time dependent inhibition variation (b) (Inset Fig. 5b indicated time-kill variation of CRA plates, the control plate shown with dark black color (a) and absence of black color in the increasing concentration (b–e)), biofilm metabolic activity (c) and decreased EPS quantification (d) of Ag NPs against *S. saprophyticus* at different concentration.

enzyme production in food borne pathogens [36].

3.12. EPS quantification assay

Disruption of EPS production in the bacteria is an important key factor to control biofilm formation [29]. Because, EPS is a polysaccharides composed of nucleic acid, protein, DNA and other leakage materials, which provide a structure to biofilm and binding sites for microorganisms [36]. It helped to bacteria in the biofilm matrix including attachment, permeation, and protection. The continuous assembling of EPS encourage the virulence of bacterial cells, making bacteria develop more resistant to antibiotics [38]. In our study, 70 and

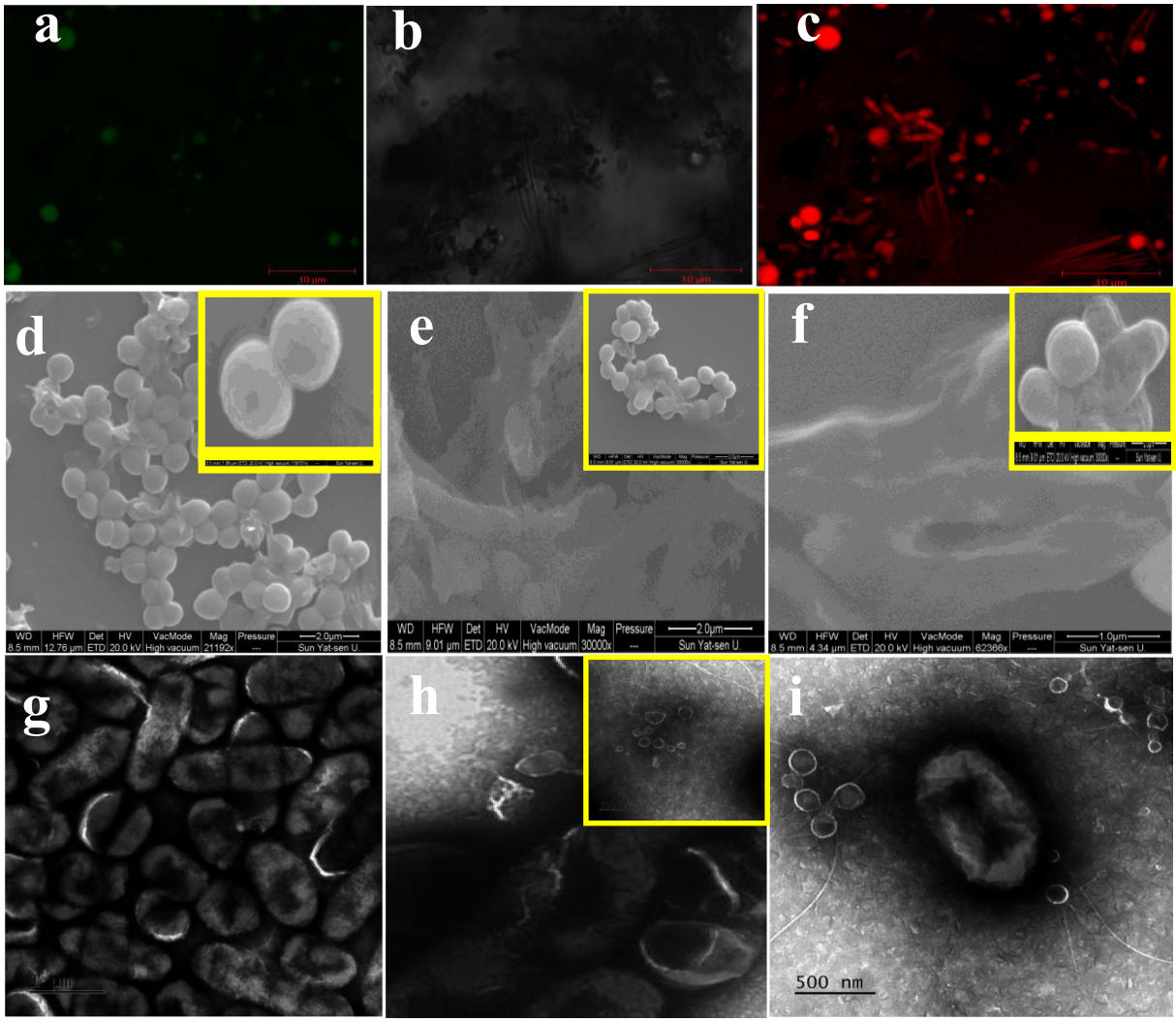

Fig. 7. Live/dead cells variation of Ag NPs untreated (a) and treated (b, c) images of *S. saprophyticus* by CLSM. Morphological damage of Ag NPs untreated (d, g) and treated *S. saprophyticus* (e, f and h, i) by SEM and TEM images.

40 μg/mL of Ag NPs exhibited 86 and 54% (Fig. 6d) decreased EPS production significantly in *S. saprophyticus* (MN310601). Previously, the binding ability of Ag NPs against bacterial surface was more in GPB of our study revealed the transaction of Ag^{+} ion into the exopolysaccharide, which is helped bacteria to develop the resistant against current antibiotics [31].

3.13. Live/dead cells differentiation

After 24 h, the damaged cell morphology of Ag NPs treated *S. saprophyticus* (MN310601) was used to stain with two nucleic acid dyes (CYTO 9 and PI) for detection of live/dead cell variations (Fig. 7). In result, green fluorescence dye CYTO 9 stain was strongly attached both treated and untreated cells representing live and dead ones. Whereas, the stain PI could only penetrated in damaged bacterial membrane. The CYTO 9 and PI stained cells were exhibited green (Fig. 7a) and red color images (Fig. 7b, c), respectively. The exhibited results were proved that the biosynthesized Ag NPs could destroy the bacterial membrane effectively. Our result was agreed by Rajivgandhi et al. [31], who reported that the Ag NPs inactivated the GPB by destroying the bacterial membrane. Damaged cell wall and cytoplasmic membrane emitted more red color due to the penetration of PI into the damaged nucleic acid cell membrane [60]. Therefore, our results suggested that the Ag NPs has more inhibition ability in cell wall and cytoplasmic membrane of *S. saprophyticus* (MN310601).

3.14. Morphological damage analysis by SEM and TEM

The morphological damage of Ag NPs treated bacterial biofilm at 24 h was clearly visualized under SEM and TEM analysis (Fig. 7). High magnification images (Fig. 7e, f) were showed with clear damage with belbing. In addition, the EPS and peptidoglycan bond layers were degraded due to the arrest of nucleic acid, protein, DNA and discharged materials. Bacterial colonization has been disrupted and somatic cell damages were found in the bacterial morphology when compared with untreated control (Fig. 7d). Inserted Fig. 7e, f proved that the Ag NPs vigorously interacted with cell wall of bacteria. The leakages of cellular material and altered bacterial shapes were clearly noticed the intracellular permeability of Ag NPs. Cell wall disruption, changed peptidoglycan layers and arrest of lipoprotein components were more evident that the Ag NPs destructed the bacterial structure. Similarly, distorted morphology of treated *S. saprophyticus* (MN310601) and smooth morphology of untreated control were differentiated by TEM result Fig. 7h, i. Therefore, both the SEM and TEM results were proved that the Ag NPs was degraded the bacterial cell wall when compared with untreated control (Fig. 7g).

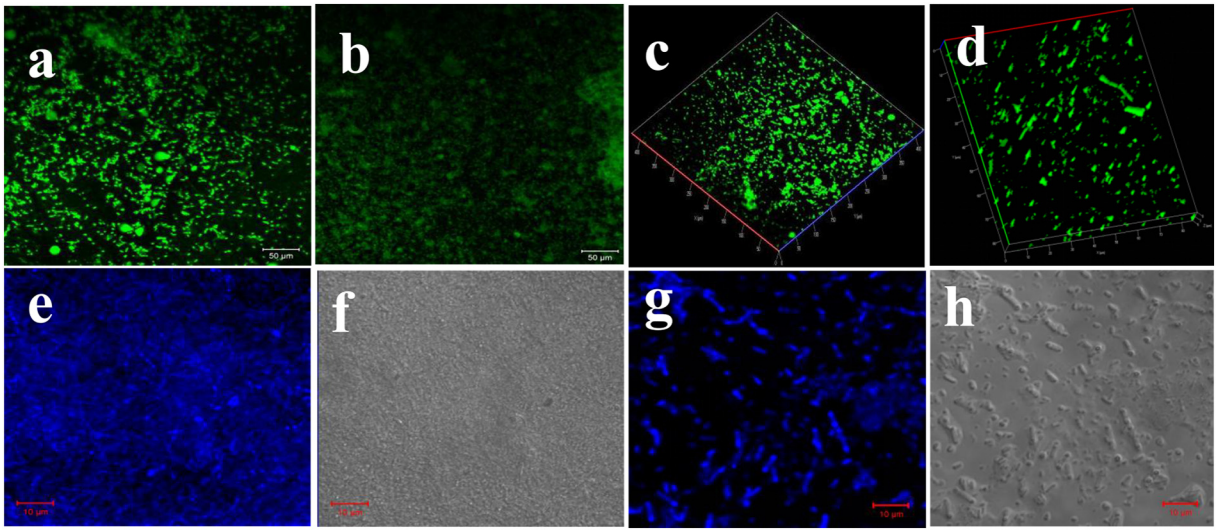

Fig. 8. The Architectural damage of biofilm in 2D and 3D of control (a, c) and Ag NPs treated (b, d) *S. saprophyticus* by CLSM using AO dye. The structural modification of untreated (e, f) and Ag NPs treated (g, h) S. saprophyticus by CLSM using DAPI.

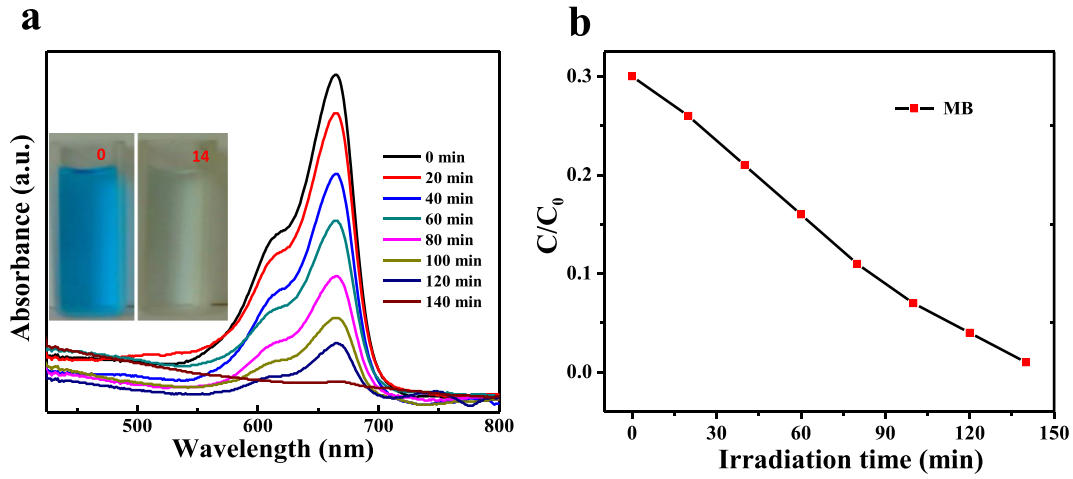

Fig. 9. The photocatalytic degradation of Ag NPs against MB dye molecules at different time interval (0–140 min) using UV–Visible absorption spectra (a) and photocatalytic irradiation of MB dye molecules in the presence of Ag NPs (b).

Table 3
Comparison of earlier reports with Ag NPs for photocatalyst determination of MB dye molecules.

Photo-catalyst	Synthesis methods	Degradation (%)	Degradation (min)	Reference
Ag NPs	Green synthesis	87	120	[23]
Ag NPs	Green and Facial synthesis	78	90	[48]
Ag NPs	Facial Green synthesis	90	200	[49]
Ag NPs	Facial synthesis	92	150	[50]
Ag NPs	Chemical synthesis	97.6	120	[51]
Ag NPs	Green synthesis	100	140	Present work

Table 4
Statistical one-way analysis of variance (ANOVA) and Turkey's Post Hoc test results of anti-bacterial and anti-biofilm activity of Ag NPs.

S.·no	Ag NPs	One-way ANOVA (level of significance) for *Staphylococcus saprophyticus* BDUMS 5
1	Minimum inhibition concentration (MIC)	0.390
2	Minimum biofilm inhibition concentration (BIC)	0.728
3	Time-Kill variation assay	0.943
3	Metabolic Activity (BIC)	0.670
4	EPS quantification (BIC)	1.000

3.15. Analysis of biofilm damage

The arrangement of extra cellular polymeric substances was collapsed due to the treatment of Ag NPs at after 24 h treatment when compared with control (Fig. 8b). The damaged structure, uncluster biofilm formation with drastically distributed arrangement of the red color biofilm structure and thick, tightly packed extra cellular components of the green cluster biofilm structure was observed in Ag NPs treated and untreated cells, respectively (Fig. 8a). Therefore, multiple layer degradation with spares cell cluster of treated cells were concluded that the Ag NPs has more anti-biofilm ability. Recently Anjugam et al. [35] reported that the large number of red florescence images were observed in uncluster treated group, indicating absence of extra cellular components materials. Mechanistically, pH insensitive molecules of the EB dye penetrated with low pH damaged biofilm structure. Because, Ag NPs and its Ag^+ ions were relatively resistant to photolabelling, which dominated AO dyes in treated cells and reduce the green color due to the ester bond breakages [31]. The 3D images of our result was agreed by Zarei et al. [61], who reported that the bacterial thickness variation was depends on the bacterial death. Inconsistent cell counts and degraded biofilm thickness was observed in the treated cells of 3D when compared to control (c, d).

3.16. Mature biofilm damage

The teichoic acid and lipoteichoic acid are two major molecules in peptidoglycan surface of GPB is an important barrier verses anti-bacterial agents, which are contributing in negative charge of this envelop. In that sense, Ag^+ ions can interact with negative charged surface ions in outer membrane of GPB and altered the functional groups of peptidoglycon. In addition, Ag NPs inhibits cell wall and bacterial growth by reduction of amino acid and protein synthesis [29]. Due to this mechanism, biofilm producing ability of bacteria was arrested. This interaction maybe related to charged particles of bacterial surface and functional groups of anti-bacterial agent. In result, PI stained membrane compromised cells were showed with red color, indicating that and more number of dead cells when compared with control (Fig. 8e, f). Therefore, these evidences proved that the Ag NPs possessed efficient ability to disrupt the membrane structure of bacteria. In addition, the identified result not only good agreement with the result obtained from PI staining, but also confirmed by DAPI staining that the biofilm structure was degraded (Fig. 8g, h). In summary, all the in-vitro study of our results were suggested that the Ag NPs has strong anti-bacterial and anti-biofilm activities when tested against *S. saprophyticus* (MN310601). Metallic nanomaterials has been reported toxic, carcinogenic and cause irritation as they become transparent to the human cell dermis. Exothermic combustion can be lead to explosion, as fine metal nanoparticles act as strong explosives. Hence, these are the very important disadvantages of metallic nanoparticle for human. The probable mechanism involved for the detection of bacterial pathogens can be attributed to disruption of cell membrane due to the release of Ag^+ ions from Ag NPs, which attached to the negatively charged microbial cell wall and rupture it, thereby caused protein denaturation and cell death. Once entered into microbial cell, it may bind to deoxyribonucleic acid molecules and involved in crosslinking of nucleic acid strands, formed a disorganized helical structure [62,63]. In addition, the zinc ion was uptake by the microbial cells and it also interrupts important biochemical processes [64].

3.17. Photocatalytic activity

The photocatalytic efficacy of the synthesized Ag NPs confirmed by means of using MB dye molecules in aqueous solution. The absorption of MB dye molecules were in the visible region at 660 nm observed in an UV–visible absorption spectrometer. The time based UV–visible absorption spectra of MB dye molecules solution in the presence of photocatalyst is showed in Fig. 8. The MB dye molecules degradation absorbance decreased with increasing irradiation time. The irradiation time differ based on the dye molecule interaction with synthesized Ag NPs. The Ag NPs reacted with MB dye molecules has 100% degradation at an irradiation time of 140 min (Fig. 9a).

The Ag NPs influenced photocatalytic degradation of MB dye molecules under light irradiation displayed in Fig. 9b. The Ag NPs exhibited innovative enhancement that was double as much improved. The above observation attributed to the inducing electron motion from the conductivity band of Ag NPs that may lessen the recombination of photocreated electron–gap pairs and as a result, the prepared Ag NPs expected to show developed photocatalytic action than other potocatalyst [65]. The MB dye molecule exhibited higher photocatalytic implementation than other dye molecules [66]. The synthesized Ag NPs exhibited the extreme performance compare to previous reported Ag NPs was attributed to the promising information. Based on our result, we have discussed some of the works related to our studies, which were published elsewhere (Table 3).

3.18. Statistical analysis

The statistical reports of all the in-vitro inhibition results were conducted one-way analysis of variance (ANOVA) and Turkey's Post Hoc test. The result was indicated as * $P \leq 0.05$ (ST. 3). All the statistical analysis results were available in Table 4.

4. Conclusion

S. saprophyticus is an important MDR bacteria, which is a dangerous since this bacterium produce enterotoxigenic. The attachment of *Saprophyticus* to food contact surface creates more problem, because virulence of this organism provide a source of contamination. Our study proved that the *S. saprophyticus* was more sensitive to Ag NPs, and it caused damage in intracellular membrane and cell wall damage at dose dependent manner. In addition, the Ag NPs has excellent photocatalytic activity to reduction of MB dye molecules. Therefore, we concluded that the biosynthesized Ag NPs was promising photocatalysis and antibacterial material through dye removal and cell cycle arrest of *S. saprophyticus*.

CRediT authorship contribution statement

Govindan Nadar Rajivgandhi: Methodology, Conceptualization, Investigation, Writing - original draft. **Muthuchamy Maruthupandy:** Methodology, Conceptualization, Investigation, Writing - original draft. **Jia-Ling Li:** Data curation, Formal analysis. **Lei Dong:** Data curation, Formal analysis. **Naiyf S. Alharbi:** Funding acquisition. **Shine Kadaikunnan:** Funding acquisition, Project administration. **Jamal M. Khaled:** Funding acquisition. **Khalid F. Alanzi:** Funding acquisition. **Wen-Jun Li:** Funding acquisition, Project administration, Resources, Software, Supervision, Validation, Visualization, Writing - original draft, Writing - review & editing.

Declaration of competing interest

All authors declare no any conflict of interest.

Acknowledgment

All the authors gratefully acknowledge the National Natural Science Foundation of China (Nos: 41950410573 and 31670009) and China Postdoctoral Science Foundation (No. 2019M663213) for financial support for this work. The authors extend their appreciation to the Deanship of Scientific Research at King Saud University for funding this work through ResearchGroup No. RG-1438- 091.

References

[1] D. Francesco, A. Mariann, S. Mariarenat, F. Giovann, Nanoencapsulation of essential oils to enhance their antimicrobial activity in foods, LWT - Food Scie. Technol. 44 (2018) 1908–1914.

[2] L. Aiping, S. Li, T. Yuxi, Z. Zhenghai, L. Yuntao, L. Cheng, Food integrity in China: insights from the national food spot check data in 2016, Food Cont 84 (2018) 403–407.

[3] X. Yan, S. Gu, X. Cui, Y. Shi, S. Wen, H. Chen, J. Ge, Antimicrobial, anti-adhesive and antibiofilm potential of biosurfactants isolated from *Pediococcus acidilactici* and *Lactobacillus plantarum* against *Staphylococcus aureus* CMCC26003, Microb. Pathog. 127 (2019) 12–20.

[4] S. Pooja, P. Raksh, G. Aniket, D. Marcos, Z. Susana, R. Mahendra, *Colletotrichum* sp.-mediated synthesis of sulphur and aluminium oxide nanoparticles and its *in vitro* activity against selected food-borne pathogens, LWT - Food Scie. Technol. 81 (2017) 188–194.

[5] S. Xiao-Hong, Z. Tong-tong, W. Cai-hong, L. Wei-qing, Z. Yong, P. Ying-jie, C.H. Vivian, Antibacterial effect and mechanism of anthocyanin rich Chinese wild blueberry extract on various foodborne pathogens, Food Cont 94 (2018) 155–161.

[6] E.A. Mohamed, Q.B. Marcos, B. Karola, C.A. Sonia, A.B. Mohamed, M.K. Rania, M.M. Abdallah, C.M. Pilar, B.V. Jorge, Molecular characterisation and typing the methicillin resistance of *Staphylococcus* spp. isolated from raw milk and cheeses in northwest Spain: a mini survey, Int. Dair. Journal 89 (2019) 68–76.

[7] S. Harakeh, H. Yassine, S. Hajjar, M. El-Fadel, Isolates of *Staphylococcus aureus* and *saprophyticus* resistant to antimicrobials isolated from the Lebanese aquatic environment, Marain Poll. Bullut. 52 (2006) 912–919.

[8] B.S.R. Jessica, T.S. Neyrijane, O.A.S. Joao, M.S. Janaína, C.L. Myrella, C.B. Regina, M. Marciane, Efficacy of using oregano essential oil and carvacrol to remove young and mature *Staphylococcus aureus* biofilms on food-contact surfaces of stainless steel, LWT 93 (2018) 293–299.

[9] R. Subbaiya, M. Saravanan, A.R. Priya, K.R. Shanka, M. Selvam, M. Ovais, R. Balajee, H. Barabadi, Biomimetic synthesis of silver nanoparticles from *Streptomyces atrovirens* and their potential anticancer activity against human breast cancer cells, IET Nanobiotechnol 11 (2017) 965–972.

[10] H. Barabadiorcid, F. Kobarfardorcid, H. Vahidi, Biosynthesis and characterization of biogenic tellurium nanoparticles by using *Penicillium chrysogenum* PTCC 5031: a novel approach in gold biotechnology, Ianian J. Pharm. Res. 17 (2018) 87–97.

[11] H. Barabadi, A. Alizadeh, M. Ovais, A. Ahmadi, Z.K. Shinwari, M. Saravanan, Efficacy of green nanoparticles against cancerous and normal cell lines: a systematic review and meta-analysis, IET Nanobiotechnol 12 (2018) 377–391.

[12] H. Barabadi, S. Honary, P. Ebrahimi, A. Alizadeh, F. Naghibi, M. Saravanan, Optimization of myco-synthesized silver nanoparticles by response surface methodology employing Box-Behnken design, Inorg. Nano-Met. Chem. 49 (2019), https://doi.org/10.1080/24701556.2019.1583251.

[13] H. Barabadi, Z. Alizade, M.T. Rahimi, A. Barac, A.E. Maraolo, L.J. Robertson, A. Masjedi, F. Shahrivar, E. Ahmadpour, Nanobiotechnology as an emerging approach to combat malaria: a systematic review, Nanomed-Nanotechnol 18 (2019) 221–233.

[14] H. Barabadi, S. Honary, M.A. Mohammadi, E. Ahmadpour, M.T. Rahimi, A. Alizadeh, F. Naghibi, M. Saravanan, Green chemical synthesis of gold nanoparticles by using *Penicillium aculeatum* and their scolicidal activity against hydatid cyst protoscolices of *Echinococcus granulosus*, Environ. Sci. Pollut. Res. 24 (2017) 5800–5810.

[15] M. Saravanan, H. Barabadi, B. Ramachandran, G. Venkatraman, K. Ponmurugane, Chapter eleven - emerging plant-based anti-cancer green nanomaterials in present scenario, Compr. Anal. Chem. 87 (2019) 291–318.

[16] M. Saravanan, T. Asmalash, A. Gebrekidan, D. Gebreegziabiher, T. Araya, H. Hilekiros, H. Barabadi, K. Ramanathan, Nano-medicine as a newly emerging approach to combat human immunodeficiency virus (HIV), Pharm. Nanotechnol. 6 (2018) 17–27.

[17] A. Khatua, E. Priyadarshini, P. Rajamani, A. Patel, J. Kumar, A. Naik, M. Saravanan, H. Barabadi, A. Prasad, L. Ghosh, B. Paul, R. Meena, Phytosynthesis, characterization and fungicidal potential of emerging gold nanoparticles using pongamia pinnata leave extract: a novel approach in nanoparticle synthesis, J. Clust. Sci. 31 (2020) 125–131.

[18] V. Manikandan, P. Velmurugan, J.-H. Park, W.-S. Chang, Y.-J. Park, P. Jayanthi, M. Cho, Oh, Green synthesis of silver oxide nanoparticles and its antibacterial activity against dental pathogens, 3 Biotech 7 (2017) 72.

[19] K. Kanagamani, P. Muthukrishnan, K. Shankar, A. Kathiresan, H. Barabadi, M. Saravanan, Antimicrobial, cytotoxicity and photocatalytic degradation of norfloxacin using Kleinia grandiflora mediated silver nanoparticles, J. Clust. Sci. 30 (2019) 1415–1424.

[20] P. Boomi, G.P. Poorani, S. Palanisamy, S. Selvam, G. Ramanathan, S. Ravikumar, H. Barabadi, H.G. Prabu, J. Jeyakanthan, M. Saravanan, Evaluation of antibacterial and anticancer potential of polyaniline-bimetal nanocomposites synthesized from chemical reduction method, J. Clust. Sci. 30 (2019) 715–726.

[21] H. Barabadi, M. Ovais, Z.K. Shinwari, M. Saravanan, Anti-cancer green bionanomaterials: present status and future prospects, Green Chem. Lett. Rev. 10 (2017) 285–314.

[22] M.T. Rahimi, E. Ahmadpour, B.R. Esboei, A. Spotin, M.H.K. Koshki, A. Alizadeh, S. Honary, H. Barabadi, M.A. Mohammadi, Scolicidal activity of biosynthesized silver nanoparticles against *Echinococcus granulosus* protoscolices, Int. J. Surg. 19 (2015) 128–133.

[23] A. Khatua, A. Prasad, E. Priyadarshini, A.K. Patel, A. Naik, M. Saravanan, H. Barabadi, L. Ghosh, B. Paul, R. Paulraj, R. Meena, Emerging antineoplastic plant-based gold nanoparticle synthesis: a mechanistic exploration of their anticancer activity toward cervical cancer cells, J. Clust. Sci. (2019), https://doi.org/10.1007/s10876-019-01742-1.

[24] M. Sundrarajan, K. Bama, M. Bhavani, S. Jegatheeswaran, S. Ambika, A. Sangili, A.P. Nithya, R. Sumathi, R, Obtaining titanium dioxide nanoparticles with spherical shape and antimicrobial properties using M. citrifolia leaves extract by hydrothermal method, J. Photochem. Photobiol. B 171 (2017) 117–124.

[25] D. Jaya Kumar, R. Jaya Santhi, Antioxidant and cytotoxic effects of hexane extract of Morinda pubescens leaves in human liver cancer cell line, Asian Pacif. Trop. Med. (2012) 362–366.

[26] S. Onitsuka, T. Hamada, H. Okamura, Perpetration of antimicrobial gold and silver nanoparticles from tea leaf extract, Colloids Surf. B Biointerf. 173 (2019) 242–248.

[27] W.M. Zhang, W. Wang, J.J. Zhang, Z.R. Wang, Y. Wang, W.J. Hao, W.Y. Huang, Antibacterial constituents of Hainan Morinda citrifolia (Noni) leaves, J. Food Sci. 81 (2016) M1192–M1196.

[28] E. Dussossoy, P. Brat, E. Bony, F. Boudard, P. Poucheret, C. Mertz, J. Giaimis, Chracterization, anti-oxidative and anti-inflammatory effects of Costa Rican noni jiuce (Morinda citrifolia L.), J. Ethnopharmacol. 133 (2011) 108–115.

[29] S. Iravani, H. Korbekandi, S.V. Mirmohammadi, B. Zolfaghari, Synthesis of silver nanoparticles: chemical, physical and biological methods, Res. Pharmaceu. Sci. 9 (2014) 385.

[30] S. Mandal, C. Rath, C.K. Gupta, V. Nath, H. Singh, Probing occurrence of phenylpropanoids in Morinda citrifolia in relation to foliar diseases, Nat. Prod. Res. 29 (2015) 535–542.

[31] G. Rajivgandhi, M. Maruthupandy, T. Muneeswaran, M. Anand, F. Quero, N. Manoharan, W.J. Li, Biosynthesized silver nanoparticles for inhibition of antibacterial resistance and biofilm formation of methicillin-resistant coagulase negative Staphylococci, Bioorg. Chem. 89 (2019) 103008.

[32] D. Jha, P.K. Thiruveedula, R. Pathak, B. Kumar, H.K. Gautam, S. Agnihotri, A.K. Sharma, P. Kumar, Multifunctional biosynthesized silver nanoparticles exhibiting excellent antimicrobial potential against multi-drug resistant microbes along with remorkable anticancerous properties, Mat. Sci. Engin. C 80 (2017) 659–669.

[33] V. Felipe, M.L. Breser, L.P. Bohl, E. Rodrigues de Silva, C.A. Morganate, S.G. Correa, C. Porporatto, Chitosan disrupts biofilm formation and promotes biofilm eradication in Staphylococcus species isolated from bovine mastitis, Int. J. Biol. Macromol. 126 (2019) 60–67.

[34] A. Kannappan, B. Balasubramaniam, R. Ranjitha, R. Srinivasan, I. A, S.V. Packiavathy, K. Balamurugan, S. K, In vitro and in vivo biofilm inhibitory efficacy of geraniol-cefotaxime combination against Staphylococcus spp, Food Chem. Toxicol. 125 (2019) 322–332.

[35] M. Anjugam, B. Vaseeharan, A. Iswarya, M. Divya, N.M. Prabhu, K. Sankaranarayanan, Biological synthesis of silver nanoparticles using β-1, 3 glucan binding protein and their antibacterial, antibiofilm and cytotoxic potential, Microb. Pathog. 115 (2018) 31–40.

[36] R. Srinivasan, K.R. Devi, A. Kannappan, S.K. Pandian, A.V. Ravi, Piper betle and its bioactive metabolite phytol mitigates quorum sensing mediated virulence factors and biofilm of nosocomial pathogen Serratia marcescens in vitro, J. Ethanopharm. 193 (2019) 592–603.

[37] G. Rajivgandhi, M. Maruthupandy, T. Veeramani, F. Quero, W.J. Li, Anti-ESBL investigation of chitosan/silver nanocomposites against carbapenem resistant Pseudomonas aeruginosa, Int. J. Biolog. Macromol. 132 (2019) 1221–1234.

[38] J. Huang, Y. Liu, I. Yang, F. Zhou, Synthesis of sulfonated chitosan and its antibiofilm formation activity against E. coli and S. aureus, Int. J. Biolol. Macromol. 129 (2019) 980–988.

[39] L. Maxine Swee, S. Yee Poi, W. Khiew, C. Siong, F. Tuen, T. Fen, K. Yih-Yih, L. Chee-Onn, Green synthesis of graphene-silver nanocomposites and its application as a potent marine antifoling agent, Collo. Surf. B:Biointerf. 148 (2016) 392–401.

[40] J.H. Zhang, H.L. Xin, Y.M. Xu, Y. Shen, Y.Q. He, Y. Hsien, B. Lin, Morinda officinalis How-a comprehensive review of traditional uses, phytochemistry and pharmacology, J. Ethanopharmacol. 213 (2018) 230–255.

[41] P. Thatoi, R.G. Kerry, S. Gouda, G. Das, K. Pramanik, H. Thatoi, J. Patra, Photo-mediated green synthesis of silver and zinc oxide nanoparticles using aqueous extracts of two mangrove plant species, Heritiera fomes and Sonneratia apetala and investigation of their biomedical applications, J. Photochem. Photobiol. B. 163 (2016) 311–318.

[42] S. Muthupandian, B. Ramachandran, H. Barabadic, The prevalence and drug resistance pattern of extended spectrum β–lactamases (ESBLs) producing Enterobacteriaceae in Africa, Microb. Pathog. 114 (2018) 180–192.

[43] V. Subramaniam, M. Adenan, A.R. Ahmad, R. Sahdan, Natural antioxidants: Piper sarmentosum (Kadok) and Morinda elliptica (Mengkudu), Malays, J. Nut. 9 (2003) 41–51.

[44] M. Bittova, D. Hladůkova, V. Roblova, S. Krácmar, P. Kubán, V. Kubán, Analysis of organic acids, deacetyl asperulosidic acid and polyphenolic compounds asa potential tool for characterization of Noni (Morinda citrifolia), Product. Nat. Prod. Communicat. 10 (2015) 1817–1820.

[45] T. Anitha, S. Mohandass, S, Anti-oxidant activity of Morinda citrifolia on lymphoma-bearing mice, Anc. Scie. of Life. 26 (2006) 85–88.

[46] M. Dadashpour, A. Firouzi-Amandi, M. Pourhassan-Moghaddam, M.J. Maleki, N. Soozangar, F. Jeddi, M. Nouri, Biomimetic synthesis of silver nanoparticles using Matricaria chamomilla extract and their potential anticancer activity against human lung cancer cells, Mat. Scie. Eng. C. 92 (2018) 902–912.

[47] S. Agnihotri, S. Mukherji, S. Mukherji, Size-controlled silver nanoparticles synthesized over the range 5–100 nm using the same protocol and their antibacterial efficacy, RSC Adv. 4 (2014) 3974–3983.

[48] S. Pal, Y.K. Tak, J.M. Song, Does the antibacterial activity of silver nanoparticles

depend on the shape of the nanoparticle? A study of the gram-negative bacterium *Escherichia coli*, Appl. Environ. Microbiol. 73 (2007) 1712–1720.
[49] G.A. Martínez-Castañón, N. Niño-Martínez, F. Martínez-Gutierrez, J.R. Martínez-Mendoza, F. Ruiz, Synthesis and antibacterial activity of silver nanoparticles with different sizes, J. Nanopart. Res. 10 (2008) 1343–1348.
[50] L. Agbaje, A.O. Sunday, M.O. Suliat, Anti-candida, anti-coagulant and thrombolytic activities of biosynthesized silver nanoparticles using cell-free extract of *Bacillus safensis* LAU 13, Process Biochem. 51 (2016) 406–1412.
[51] S. Goyal, N. Gupta, A. Kumar, S. Chatterjee, S. Nimesh, Antibacterial, anticancer and antioxidant potential of silver nanoparticles engineered using *Trigonella foenum-graecum* seed extract, IET Nanobiotechnol 12 (2018) 526–533.
[52] K. Venugopal, H. Ahmad, E. Manikandan, K. Thanigai Arul, K. Kavitha, M.K. Moodley, K. Rajagopal, R. Balabhaskar, M. Bhaskar, The impact of anticancer activity upon Beta vulgaris extract mediated biosynthesized silver nanoparticles (ag-NPs) against human breast (MCF-7), lung (A549) and pharynx (Hep-2) cancer cell lines, J. Photochem. Photobiol. B 173 (2017) 99–107.
[53] L. Rufen, C. Zhen, R. Na, W. Yixuan, W. Yujia, Y. Fengye, Y, Biosynthesis of silver oxide nanoparticles and their photocatalytic and antimicrobial activity evaluation for wound healing applications in nursing care, J. Photochem. Photobiol. B 199 (2019) 111593.
[54] D. Ayse, Y. Vedat, I. Nilay, O. Baldemir Ismail, Anthocyanins-rich berry extracts directed formation of Ag NPs with the investigation of their antioxidant and anti-microbial activities, J. Molecul. Lipids. 248 (2017) 1044–1049.
[55] R. Balachandar, P. Gurumoorthy, N. Karmegam, H. Barabadi, R. Subbaiya, K. Anand, P. Boomi, M. Saravanan, Plant-mediated synthesis, characterization and bactericidal potential of emerging silver nanoparticles using stem extract of *Phyllanthus pinnatus*: a recent advance in phytonanotechnology, J. Clust. Sci. 30 (2019) 1481–1488.
[56] G. Arya, R.M. Kumari, N. Sharma, N. Gupta, A. Kumar, S. Chatterjee, S. Nomesh, Catalytic, antibacterial and antibiofilm efficacy of biosynthesised silver nano-particle using *Prosopis juliflora* leaf extract along with their wound healing potential, J. Photochem. Photobiol. B 190 (2019) 50–58.
[57] D. Pratik, G. Krishanu, J. Nandan Kumar, M. Anwesh, B. Piyali, Green synthesis and characterization of silver nanoparticles using belladonna mother tincture and its efficacy as a potential antibacterial and anti-inflammatory agent, Mat. Chem. Phy. 228 (2019) 310–317.
[58] K. Steff, G. Shanthi, A.S. Maroky, S. Selvakumar, Enhanced antibacterial effects of green synthesized ZnO NPs using *Aristolochia indica* against multi-drug resistant bacterial pathogens from diabetic foot ulcer, J. Inf. Publ. Heal. 11 (2018) 463–471.
[59] T.Y. Suman, S.R. Radhika Rajasree, A. Kanchana, S.B. Elizabeth, Biosynthesis, characterization and cytotoxic effect of plant mediated silver nanoparticles using *Morinda citrifolia* root extract, Coll. Surf. B Biointerf. 106 (2013) 74–78.
[60] D. Nayak, S. Pradhan, S. Ashe, P.R.S. Rauta, B. Nayak, Biologically synthesised silver nanoparticles from three diverse family of plant extracts and their anticancer activity against *epidermoid* A431 carcinoma, J. Collo. Interf. Sci. 457 (2015) 329–338.
[61] M. Zarei, A. Jamnejad, E. Khajehali, Antibacterial effect of silver nanoparticles against four foodborne pathogens, Jund. J. Microb. 7 (2014) e8720.
[62] I. Chanu, P. Krishnamurthi, P.T. Manoharan, Effect of silver on plasmonic, photocatalytic, and cytotoxicity of gold inauagzno nanocomposites, J. Phys. Chem. C 121 (2017) 9077–9088.
[63] A. Lipovsky, Z. Tzitrinovich, H. Friedmann, G. Applerot, A. Gedanken, R. Lubart, EPR study of visible light-induced ROS generation by nanoparticles of ZnO, J. Phys. Chem. C 113 (2009) 15997–16001.
[64] D.A. Lyons, W.S. Talbot, Targeting mechanisms in myelinated axons: not all nodes are created equal, Dev. Cell 22 (2012) 7–9.
[65] Z.U. Khan, H.M. Sadiq, N.S. Shah, A.U. Khan, N. Muhammad, S. Hassan, U. Tahir, Greener synthesis of zinc oxide nanoparticles using *Trianthema portulacastrum* extrcat and evaluation of its photocatalytic and biological applications, J. Photochem. Photobiol. B 192 (2019) 147–157.
[66] P. Sentil kumar, G. Yaswant, S. Kavitha, E. Chandramohan, G. Kowsalya, R. Vijay, B. Sudhagar, Preperation and characterization of hybrid chitosan-silver nanoparticles (Chi-Ag NPs); a potential antibacterial agent, Int. J. Biolog. Macromol. 141 (2019) 290–298.